Diploma Thesis

Development of Fast Chromatography Based on a Negative Thermal Gradient-GC for the Study of Volatile Products Formed in Lithium-Ion Batteries

Conducted for the purpose of obtaining the academic degree of
Diplom-Ingenieur in Technical Chemistry at

Vienna University of Technology
Institute of Chemical Technologies and Analytics

under the supervision of
Ao. Univ. Prof. Dipl.-Ing. Dr. techn. Egon Erwin Rosenberg
Projekt-Ass. Dipl.-Ing. Bernhard Klampfl

by
Sebastian Woehrer BSc
11738826

Vienna, December 2023

Acknowledgements

First of all I want to thank the FFG for the funding of the OPERION project (879613) providing the necessary funds for this thesis.

I want to thank my supervisor Erwin Rosenberg for having me in his research group and for always listening to me and giving input when I had problems. Also a big thank you is owed to all members of the research group making my stay as pleasant as possible. Additionally, I want to thank Juergen Kahr and Christiane Groher from AIT whose friendliness and hospitality always made me feel welcome when doing experiments in their lab.

I owe a big thank you to my good friend and supervisor Bernhard who was not only there for me when having troubles with the experiment but also when the burdens of doing my thesis while working as lab tutor and doing exams seemed unmanagable. I will never forget our adventures in the lab and "in-silico" while trying to overcome a zombie apocalypse until late in the night.

I want to thank my dear friends Clemens, Miranda, Kopi, Conny, Adea, Basti, Schnölli, Edma, Michi, Geri, Peter, Jana, Felix, Markus, Moritz, Lena, Elisabeth, Hong, Rares and Leonard for making the past five years ones of the best of my life. I am not sure if I had ever gotten so far without your support and friendship.

I want to thank Irina for always being there for me and helping me keep my sanity while trying to manage writing this thesis and doing the last exams while the deadline for my PhD was coming closer and closer. Without your support and love the distress would have been a lot harder to overcome.

Last but not least I want to thank my parents who supported me not just financially over the course of my studies but also mentally by always listening to me when I had problems.

I want to thank Ufuk.

Eidesstattliche Erklärung: Ich erkläre hiermit an Eides statt, dass ich die vorliegende Arbeit selbstständig verfasst, andere als die angegebenen Quellen/Hilfsmittel nicht benutzt, und die den benutzten Quellen wörtlich und inhaltlich entnommenen Stellen als solche kenntlich gemacht habe.

Statutory declaration: I hereby declare that I have authored this thesis independently, that I have not used other than the declared sources/resources, and that I have explicitly marked all material which has been quoted either literally or by content from the used sources.

Abstract

Global efforts focus on improving lithium-ion batteries (LIBs) through electrolyte optimization and developing a deeper understanding of degradation and stabilization mechanisms. Real-time (operando) methods are crucial for investigating in-situ electrolyte degradation and aging and quantifying gas species during LIB use.

The slow heating and cooling rates of conventional temperature programmed gas chromatographs (TPGC) limit them to one run every ∼30 minutes. To expedite, sampling shortening the column is necessary, leading to reduced retention times, however, at the price of reduced resolution. Optimal separation with reduced runtime is achieved using a negative thermal gradient, enhancing analyte band resolution through peak focusing at the elution point. Three experimental setups with different GCs and detectors (FID, MS, BID) were developed and evaluated for rapid measurements, creating spatially resolved thermal gradients by cooling a resistively heated steel capillary with decreasing airflow.

Performance evaluation included measuring a C_8-C_{20} standard, resolved by two of the three systems in under 30 seconds. Additionally, chromatograms were simulated and compared to experimental results to identify setup weaknesses.

Initially in-situ use of the TGGC setup was planned by establishing a connection to the battery abuse chamber. Unfortunately, the instrument was not available until the end of this thesis. To replace online measurements during LIB cycling tests, a dynamic experiment tracked the hydrolysis of an ethylene carbonate/diethyl carbonate electrolyte sample in a headspace vial. Thereby it was shown that the instrument is able to perform measurements every 3-4 minutes. In contrast, the current GC-MS setup takes $\sim$ 30 minutes per measurement. Implementing the system online would lead to $\sim$ tenfold reduction of measurement time, significantly enhancing time resolution.

Kurzfassung

Es besteht weltweites Bestreben, die Zellchemie und Leistung von Lithium-Ionen-Batterien (LIBs) zu verbessern. Zu diesem Zweck ist es notwendig, ein besseres Verständnis über die Alterungs- und Abbauprozesse des Elektrolyten in LIBs zu erlangen. Hierfür sind Methoden mit hoher Zeitauflösung essentiell, um Gasspezies, die während des Betriebs von LIBs gebildet werden, zu identifizieren und zu quantifizieren.

In der konventionellen temperaturprogrammierten Gaschromatographie (TPGC) wird die Trennsäule, konvektiv, in einem Ofen beheizt, was zu sehr langsamen Aufheiz- und Abkühlraten und somit langen Messzeiten führt. Eine Möglichkeit zur Reduktion der Messdauer liegt in der Verkürzung der Säule, wobei Auflösung sowie Kapazität kompromittiert werden. Um bei geringerer Säulenlänge optimale Trennbedingungen beizubehalten, wird ein negativer Temperaturgradient entlang der Säule eingeführt, der die Auflösung der Analytbanden durch Peak-Fokussierung am Elutionspunkt verbessert. Drei experimentelle Aufbauten mit verschiedenen Gaschromatographen und Detektoren wurden entwickelt. Die hierfür erforderlichen räumlich aufgelösten Temperaturgradienten wurden erzeugt, indem eine widerstandsbeheizte Stahlkapillare mit einem kontrollierten Luftstrom unterschiedlich stark gekühkt wurde.

Die Testung der Systeme umfasste Messungen eines n-C_8 - n-C_{20} Standards, den zwei der drei Systeme in weniger als 30 Sekunden auflösten. Weiters wurde eine Simulation der Messungen durchgeführt und diese mit den experimentellen Ergebnissen verglichen. So konnten in den Messungen auftretende Phänomene erklärt, sowie Schwächen an der Apparatur identifiziert werden.

Ursprünglich war geplant, die getesteten experimentellen Aufbauten direkt in die Zyklisierungsversuche von LIBs einzubinden, um so on-line in-situ Messungen der gebildeten Gasspezies durchzuführen. Da die Messstelle jedoch bis Ende dieser Arbeit nicht verfügbar war, dafür wurde alternativ die Hydrolyse einer Elektrolytprobe aus Ethylencarbonat/Diethylcarbonat in einem Headspace Vial verfolgt, wobei alle zehn Minuten Proben aus dem Gasraum entnommen und gemessen wurden. Die Datenaufzeichnung hätten alle 3-4 Minuten stattfinden können, limitierender Faktor war hierbei die Equilibrierung der Gasphase im Headspace Vial. Im Gegensatz dazu benötigt das aktuelle GC-MS Setup $\sim$ 30 Minuten pro Messung. Die on-line Implementierung des Systems würde die Messzeit um einen Faktor von etwa 10 verkürzen und somit die Zeitauflösung erheblich verbessern.

Contents

1 Introduction

1.1 OPERION Project

The aim of the project OPERION is to deepen the understanding of degradation mechanisms of the cell chemistry of generation 3 cells while in use. Performing charging experiments utilizing charging rates of up to 3.5 C requires fast in-situ and on-line measurements. This can either be accomplished by performing e.g. on-line spectroscopy or fast gas chromatography. In the scope of this project, an existing gas chromatography system coupled to a mass spectrometric detector should be adapted and equipped with a negative thermal gradient gas chromatograph. This should enable the observation of cell decay processes with high temporal resolution (analysis time of one minute). In this context, different electrolyte compositions are electrochemically tested to minimise their influence on electrolyte decomposition, while gas measurements are performed simultaneously. In this way, the electrolyte can be optimised quickly and efficiently, which has a positive effect on the development time of batteries. The determination of the gas quantities enables the creation of an electrochemical, transient model to simulate the electrolyte decomposition. This model is used in combination with post-mortem analyses and operando gas measurements to investigate the decomposition mechanisms of an entire cell. This data forms the basis for making improvements to the electrolyte and/or materials on the one hand and for assessing the condition of the cell in terms of safety, service life and toxicity on the other. [1]

The acquired data is also important for the creation of a detailed Life Cycle Assessment (LCA) database as part of the project. The quantitative data from the gas analysis supplements the LCA model with an end-of-life scenario at screening level or is used to assess recyclability.[1]

The project combines the research contributions from three different the research areas:

- Development of a gas chromatograph for faster separation of complex gas mixtures utiliziting chromatography with improved time resolution resulting in a higher sample throughput. (TU Wien)
- Improving the energy density and service life of cells by optimising the electrolyte to reduce degradation effects performed by the Austrian Institute of Technology (AIT).
- Investigation of decomposition processes in lithium-ion batteries under normal

and extreme operating conditions by gas analysis using an operando fast-GC-MS, as well as the structural and chemical post-mortem characterisation of electrochemically tested electrode materials (performed by AIT and TU Wien).

- Application of an electrochemical transient model to simulate the rates and stoichiometry of electrolyte decomposition.(AVL List)
- Carrying out life cycle analyses to estimate the ecological footprint and risk assessment for cell chemistries. This task is performed by Daxner & Merl GmbH.

1.2 Aims of the Thesis

This work was carried out under the OPERION project so its main goals were aligned with the ones of the project. The first aim is to enhance the design of the peripheral electronics of the cooling tower module presented in [2] and thereby develop a "plug and play" concept type of module easily usable for anyone.

Furthermore, the understanding of the cooling tower should be deepened by performing a simulation of the n-octane to n-eicosane measurements done with this setup to detect shortcomings in the instrument and to explain upcoming phenomena in the course of the experiments. (Section 5)

Additionally, in preparation for the use with the GC-MS system at AIT, the adaptability of the cooling tower setup should be shown by connecting it to various gas chromatographs and detectors, especially to a mass spectrometric detector, and evaluating its performance.(Sections 4 to 8)

Finally, a system consisting of a gas chromatograph, the cooling tower and a detector should be adapted for in situ use in charging cycles of lithium-ion batteries (pouch cells in particular) to acquire time-resolved information with regard to degradation mechanisms in electrolytes.

2 Theoretical Background

2.1 Lithium-Ion Batteries

Figure 1 illustrates the fundamental operating principle of a lithium-ion battery. It features an ion-conducting electrolyte that contains a dissociated lithium-containing salt dissolved in for example ethylene carbonate and diethyl carbonate between two electrodes. Additionally a porous membrane acts as a separator by electrically isolating the two electrodes. Individual lithium ions move between the electrodes during charging and discharging, becoming intercalated into the active materials. While discharging, as lithium is extracted from the negative electrode (with copper serving as the current collector), electrons are liberated. The cathode typically contains active materials such as mixed oxides. For example mixed oxides of nickel, manganese and cobalt (NMC) can be used to replace as much cobalt as possible due to its inhumane extraction conditions. Batteries using these cathodes are called NMC-batteries where the number after it e.g. NMC811 stands for the different mixing ratios of the oxides. The anode is mainly composed of graphite and amorphous carbon compounds. This process is reversed when charging occurs. These materials are used to produce different kinds of cell geometries such as prismatic, cylindrical or pouch cells. The latter is depicted in Figure 2.[3, 4]

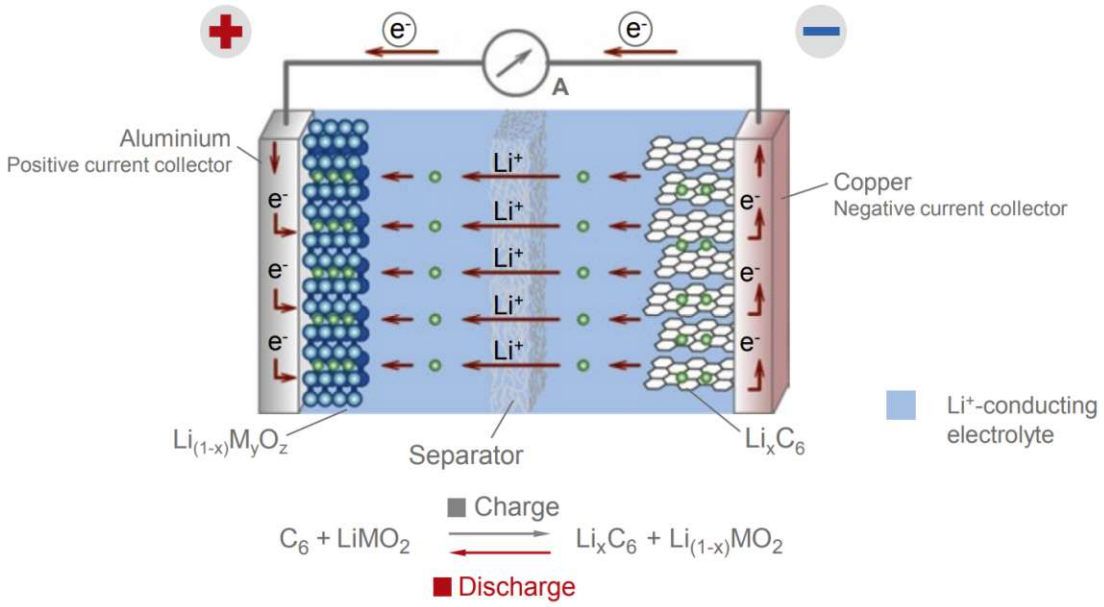

Figure 1: Processes of charging and discharging in lithium-ion batteries [4].

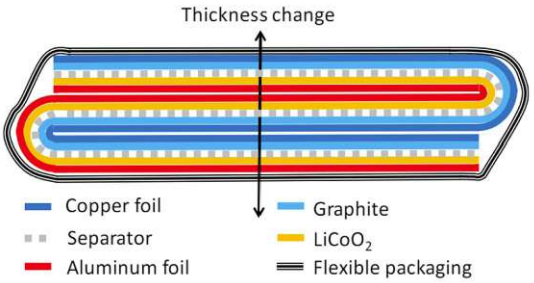

Figure 2: Schematic picture of the layers of a pouch cell [5].

2.2 Gas Chromatography

In gas chromatography (GC) the analytes are, as in liquid chromatography (LC), absorbed (partitioned) and adsorbed on the stationary phase. The analytes differ in retention times in the column due to different interactions with the stationary phase. As a mobile phase different gases e.g. H_2, He or N_2 are used. It is of significant importance that the chosen carrier gas does neither interact with the analyte molecules nor is changed in the course of analysis. The potency of the separation system is predominantly dependent on the temperature, the flow rate of the mobile phase an the length of the column. By varying these parameters the separation process can be optimised. In gas chromatography capillary columns containing bulk or liquid phases (e.g. polysiloxanes) are most commonly used. Which is particularly important for absorption and partition equilibrium. Additionally, substances with a large active surface are used, with the most common being active charcoal, alumosilicates or zeolithes, whose surfaces can be chemically modified for specific purposes. [6, 7]

The retention time in a given separation system provides qualitative information which is used to identify a specific analyte, whereas the peak area or the peak height are used for quantification. Various detectors can be used with GC such as the flame ionization detector (FID), the (BID) or the mass spectrometer.[6, 7]

2.3 Instrumentation for Conventional Gas Chromatography

Gas chromatography is mostly used for the analysis of organic compounds and finds its main fields of operation in analytical chemistry and environmental chemistry. Some of its main features are high separation efficiency and low detection limits (when coupled with a suitable detection unit). The requirement for a component for being analzed using gas chromatography is it being able to be vaporized without degrading at temperatures up to 450 °C. [8, 7]

Figure 3 shows a schematic picture of a conventional gas chromatograph. It consists a carrier gas supply, a pressure regulator, a flow controller, a sample injection port (for introduction of the sample), an oven which is housing the column, a detector and a data processing unit.

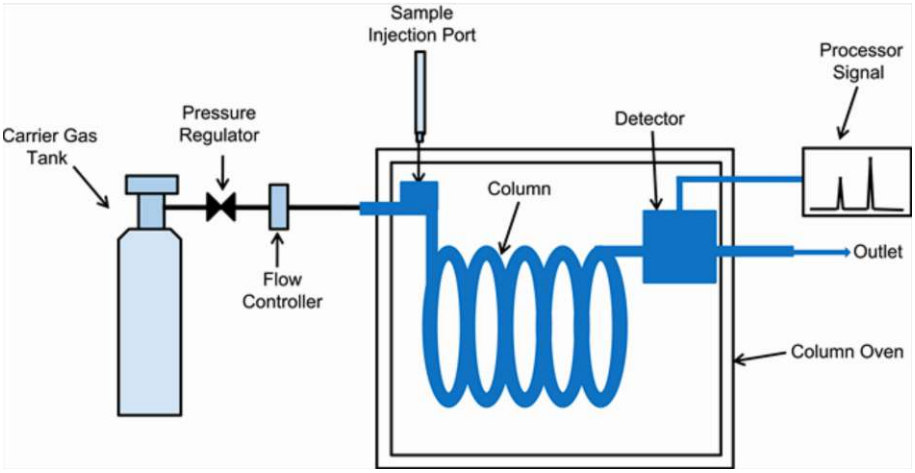

Figure 3: Schematic picture showing all necessary parts of a gas chromatograph [9].

2.4 Modi of Operation in Gas Chromatography

One of the most important aspects in gas chromatography is to perform the best possible separation in the shortest possible time span. The time required for a measurement depends on the type of column (and its stationary phase), the set flow rate of carrier gas, the choice of carrier gas itself and lastly the temperature of the column. Different modi of operation can be classified in gas chromatography and are explained in the following sections.[10, 11, 12]

2.4.1 Isothermal Gas Chromatography (ITGC)

In Isothermal Gas Chromatography (ITGC) the temperature of the column is held at a fixed constant value throughout the whole measurement time meaning that the temperature is neither variable in time nor in space. This technique is used for separating and analyzing compounds having a narrow distribution of boiling points where the introduction of a temperature ramp would result in loss of resolution. However, if the range of boiling points for the analytes of interest is significant, major drawbacks occur with this method.[10, 11, 12]

Using a higher temperature for the measurement will result in less volatile compounds eluting earlier, reducing measurement time. Unfortunately, as a result more volatile compounds may not be sufficiently separated. In turn, setting a lower tem-

perature will lead to a satisfactory result for volatile compounds but less volatile compounds will show wider peaks and higher retention times resulting in longer measurement times meaning that for efficient analysis different measurement parameters should be used to cover a wide range of compounds. This is known as the "General Elution Problem" applicable to liquid and gas chromatography. In liquid phase it is solved by introducing a solvent gradient in the mobile phase while in gas chromatography a temperature gradient is implemented resulting in Temperature Programmed Gas Chromatography.[10, 11, 12]

2.4.2 Temperature Programmed Gas Chromatography (TPGC)

TPGC utilizes a time dependent temperature gradient over the course of the measurement. For the separation of the more volatile compounds the temperature is held at lower temperature at the beginning and consequently increased to enable elution of less volatile compounds while also reducing their respective peak widths enhancing sensitivity. This results in an overall reduction in measurement time. Another advantage of this method is that it enables including a heat-out step for cleaning of the column. TPGC is the most commonly used mode of operation in gas chromatography.[10, 11, 12]

2.4.3 Thermal Gradient Gas Chromatography (TGGC)

Thermal Gradient Gas Chromatography (TGGC) is in contrast to ITGC and TPGC a rather novel operational mode in gas chromatography. If one recalls from the previous sections, ITGC holds the temperature constant over time and space, while TPGC introduces a time dependence of the temperature meaning that the temperature $T = f(t)$. In TGGC this dependence does not only apply for dimension of time but also for the dimension of space meaning that a temperature gradient along the axial column length is implemented so that $T = f(t,x)$ with x being the position along the column. Another contrast to TPGC is that the temperature gradient is negative resulting in a colder area at the end of the column than at the beginning of the column. This results in a peak focussing effect since analytes are slowed down towards the end of the column while parts of the analyte band are still in hotter parts of the column and therefore travel faster.[12, 13] This phenomenon is illustrated in Figure 4.

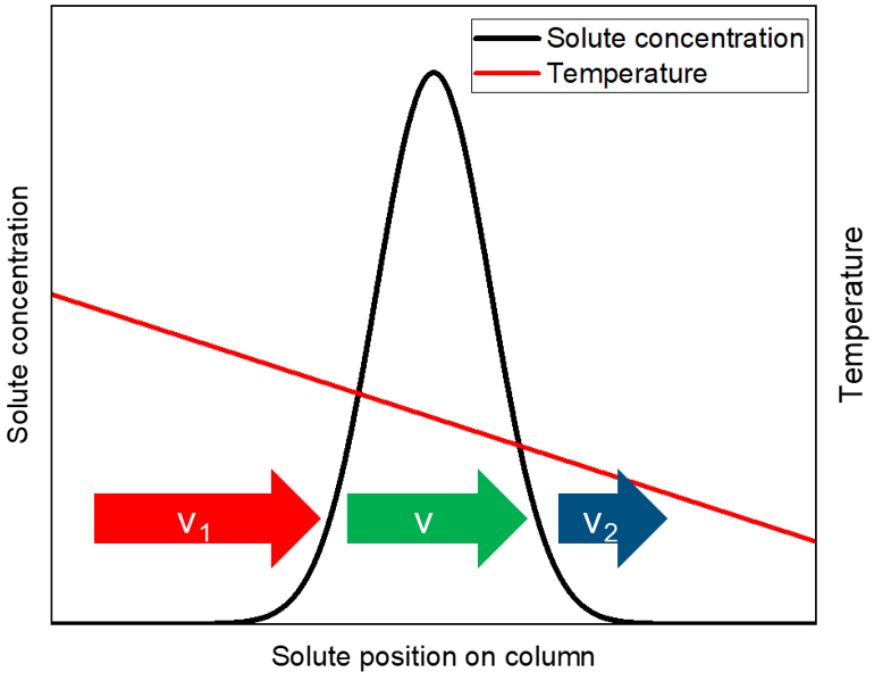

Figure 4: Schematic picture explaining the resulting peak focussing effect due to the negative thermal gradient along the column [14].

TGGC can further be categorized in stationary TGGC, where the temperature gradient does not change as a function of time, and in moving TGGC where the temperature gradient changes as a function of time. Due to its, nature TGGC can be used in fast and even hyperfast chromatography as shown by Boeker et al. [15], for continous sample introduction (shown later in this section by Contreras et al. [16] and analytes susceptible to thermal degradation are analyzable due to lower thermal stress resulting from colder elution tempeatures. [17]. All operational modi are summarized in Table 1. Instrumentation of conventional is not suitable for performing measurements using temperature gradient gas chromatography which is why a lot of focus was put in developing setups and modules able to perform stable runs with TGGC. Figure 5 shows the possibilities for creating the temperature gradient along the column.[10, 11, 12]

Table 1: Classification of operational modes in gas chromatography by their temperature dependence on time and space, with x being the axial position along the column and t representing the time.

Mode of Operation	T = f(t)	T = f(x)
ITGC	×	×
TPGC	✓	×
TGGC	×	✓
TGGC	✓	✓

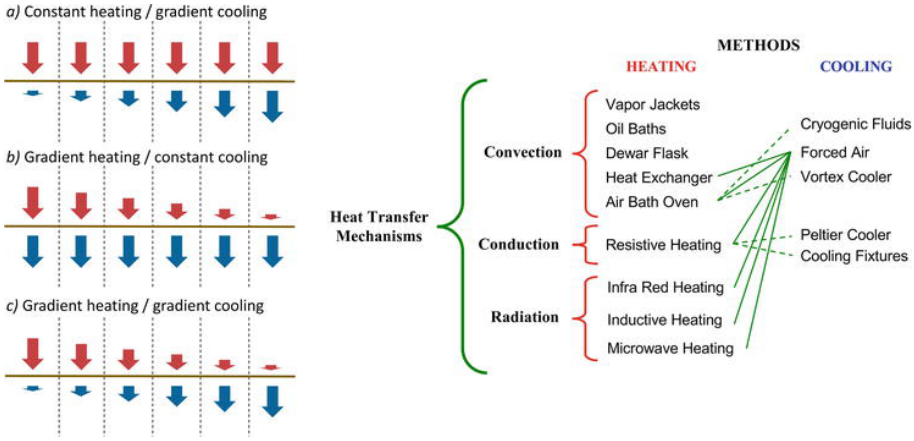

Figure 5: Possible ways of achieving a thermal gradient, taken from [12], after Contreras [16].

2.5 Negative Thermal Gradient Gas Chromatography

2.5.1 Chronology of Instrumentation for TGGC

The earliest reports of instrumentation for TGGC start in the 1950s by Zhukhovitskii utilizing mobile GC ovens for generating the temperature gradient along the column. These techniques lost their relevance with the advent of the capillary column (now the most commonly used column type in gas chromatography) due to them being significantly longer than their predecessors, the packed columns.[12, 18]

Vergnaud and Fatscher introduced a new method for generating temperature gradients in the early 1970s. This started the transition from "chromathermography" to TGGC where the temperature gradient extended along the whole column (which was still shorter than usual in a range between ∼2-5 meters. This gradient was created using a heating wire wrapped around the separation column which was then heated resistively. The number of coils per unit determined local heating of the column, thus creating the linear thermal gradient. [12, 18, 19]

Fenimore et al. [20] were the first ones to use a capillary column for use with TGGC. For their experimental setup sectional heaters made out of brass tubes with an outer diameter of 4.45 cm and a wall thickness of 0.32 cm were used. One of these units could fit 2.25 m of capillary and five of these heating sections were then joined with steel spacers between them for thermal isolation. In total they applied the thermal gradient to an 11 meter long capillary column which they were able to separate n-decane to n-octadecane within a time span of 2.4 minutes. [12, 20]

In 1991, Rubey and colleagues presented their utilization of a TGGC-system incorporating a column-sheath assembly. In this setup, nitrogen gas was directed through

the sheath, and during this passage, it underwent cooling. Inside the sheath, the gas underwent a temperature rise by being resistively heated while traversing the sheath. This instrument achieved temperatures ranging from -100 to 400 °C. Subsequently, an open tubular capillary column was placed within the sheath. Notably, the carrier gas flowed in the opposite direction to the nitrogen gas within the sheath, resulting in a negative thermal gradient along the length of the column. Rubey acknowledged that the temperature drop in this apparatus was significant and suggested that future designs should incorporate a more gradual temperature decrease. The system proposed is depicted in Figure 6.[12, 13]

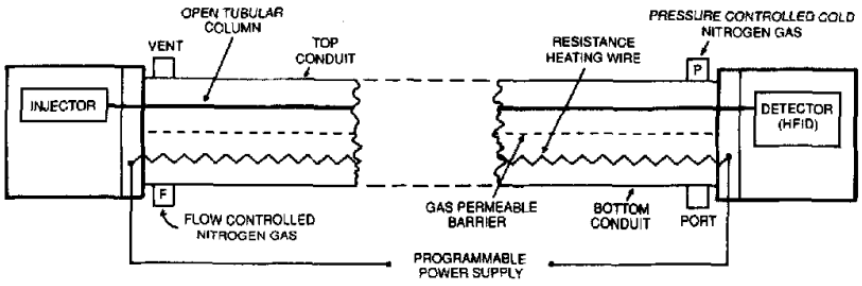

Figure 6: Realization of TGGC shown by Rubey et al. in [13]

Furthermore Rubey et al. published yet another paper with another realization of TGGC in which the column was wrung around the sheath assembly. Rubey not just only presented two new ways of performing TGGC, he also introduced the three dimensional view of the temperature being a function of time and the axial position on the column as mentioned in section 2.4.3 and, additionally, to separate n-alkanes of highly different volatilites in a time frame of 100 seconds.[12, 13, 21]

In 1995 Jain and Phillips published a series of papers in which they took advantage of resistively heating the column, reducing the required electrical power and reducing some limitations in temperature control. For applying current the columns were painted with a very thin layer of paint having electrically conductive properties. By changing the current over time a gradient was introduced. A sketch of the instrument used is presented in Figure 7. The implemented negative thermal gradient resulted in refocused analyte bands and thereby sharper and taller peaks. [12] Using this setup, the authors were able to separate n-Octane to n-decane within four seconds, with all peaks showing baseline separation. Furthermore, a mixture containing 13 compounds was separated in less than 3.5 seconds in a continouous sample stream.[22] In conclusion of their paper series, the authors stated that their technique is suitable for real-time monitoring and field measurements. [22, 23, 24]

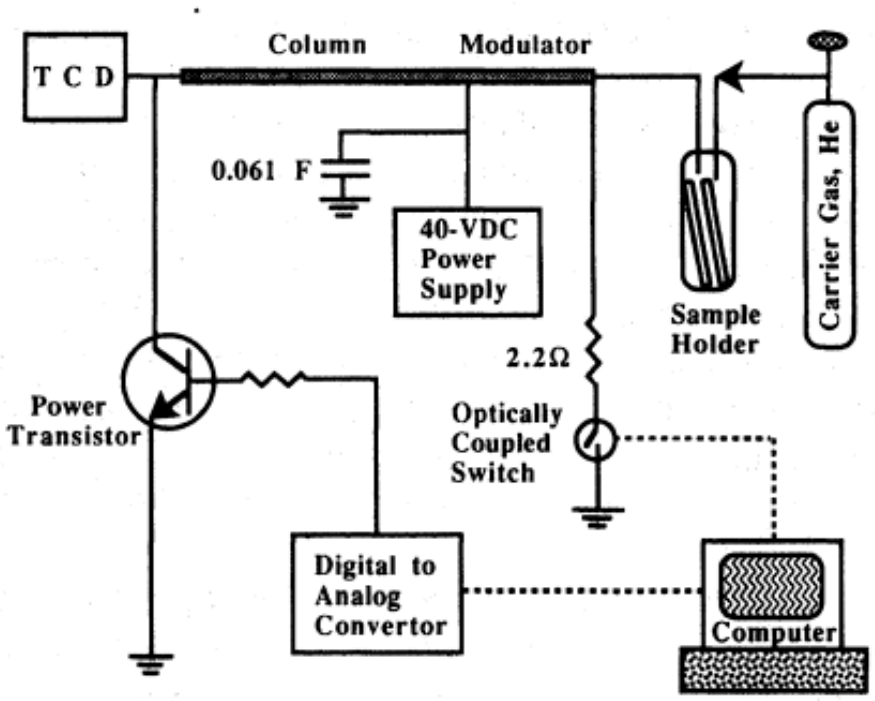

Figure 7: Sketch of the setup used in Jain and Phillips [23].

The submission of Contreras's master thesis [25] at the University of Dayton in 2004 strongly influenced developments in thermal gradient gas chromatography. It focused on the *Design and application of thermal gradient programming techniques for use in multidimensional gas chromatography-mass spectrometry (MDGC-MS)* [25]. Here TGGC was utilized as a means of focusing analyte bands moving from the first to the second column in multidimensional gas chromatography. Again a sheath assembly was used which enabled the creation of an axial temperature gradient along the column including both, fast heating and fast cooling cycles, maintaining a stationary thermal equilibrium. The assembly was installed inside the column oven which directly performed as heat source. Utilizing this system a MDGC-MS was built, in which the TGGC was used in the second dimension. The constructed sheat assembly is shown in Figure 8.[25]

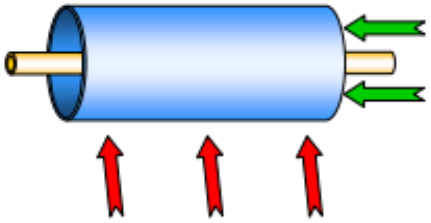

Figure 8: Sheath assembly by Contreras [16]. The green arrows represent the cooling gas flow while the red arrows stand for the heat flow directly coming from the column oven.

Contreras continued his work on thermal gradient gas chromatography in his PhD thesis at Brigham Young University which was published in 2010.[16] In this work he introduced three different models for TGGC of which one was quite similar to the column sheath assembly mentioned before.[25] The quintessential difference was that instead of using the column oven as a heating supply direct heating (in form of resistive heating) was used enabling access to different modes of operation and allowing easier manipulation of the TGGC temperature profile. The apparatus designed for this purpose is shown in Figure 9. Futhermore, he experimentally juxtaposed ITGC, TPGC and TGGC leading to the following outcome : when using the same column length TGGC is equivalent to TPGC with the only difference being that in TGGC the eluting peaks are narrower and the signal-to-noise ratio (SNR) could be increased. Experimentally it was shown that a concave down profile resulted in more volatile compounds eluting closer together while the opposite was true for less volatile compounds. In fact, the less volatile compounds were also further apart than in the convex (= concave up) measurements. These results lead them to conclude that for analyzing a mixture of compounds containing a larger number of less volatile analytes a concave (= concave down) profile should be considered for the measurements. If the opposite is the case, meaning more substances with a lower boiling point are present, a concave profile should be applied to the TGGC module. With this Contreras also showed the easy adaptability of this setup for varying sample compositions.[16]

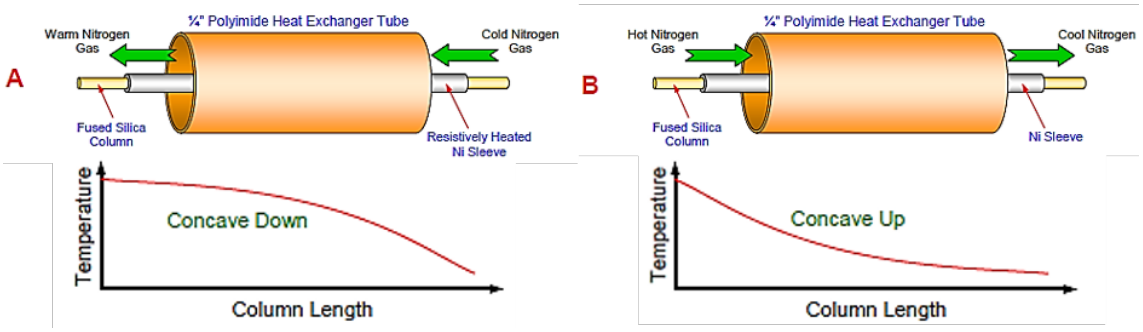

Figure 9: Heat exchanger presented in [16] for enabling concave (= concave down) temperature profiles (a) and convex (= concave up) temperature profiles (b).

A third approach for TGGC was presented in both, Contreras's PhD thesis [16] and later in a paper [26] in 2013. The new system incorporated both the fast resistive heating and the convective cooling. With this approach he aimed for introducing some flexibility in shaping the temperature profile along the column. For this purpose he placed two meters of a capillary column into a nickel tubing which he divided into 40 zones each being able to be heated and adressed separately. The resistively heated wire was wrapped around the nickel sleeve for each and every zone. A close up of the heating zones is shown in Figure 10. For cooling five PC fans were used. With this setup he was able to finely tune the temperature profiles for dynamic TGGC. This ability to influence the temperature profile allows one to optimize and impact separation efficiency. Unfortunately, the energy demand and the requirement for space (see Figure 11) make it impractical for routine use, in spite of its marvellous chromatographic capabilities.[12, 16, 26]

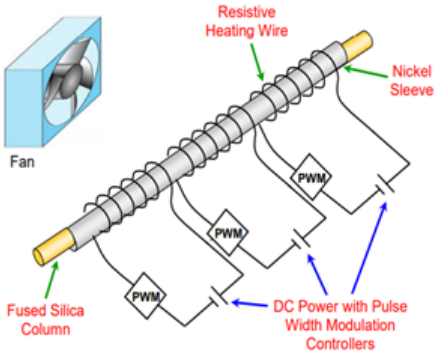

Figure 10: Close up on the resistively heated zones of the setup shown by Contreras in [16].

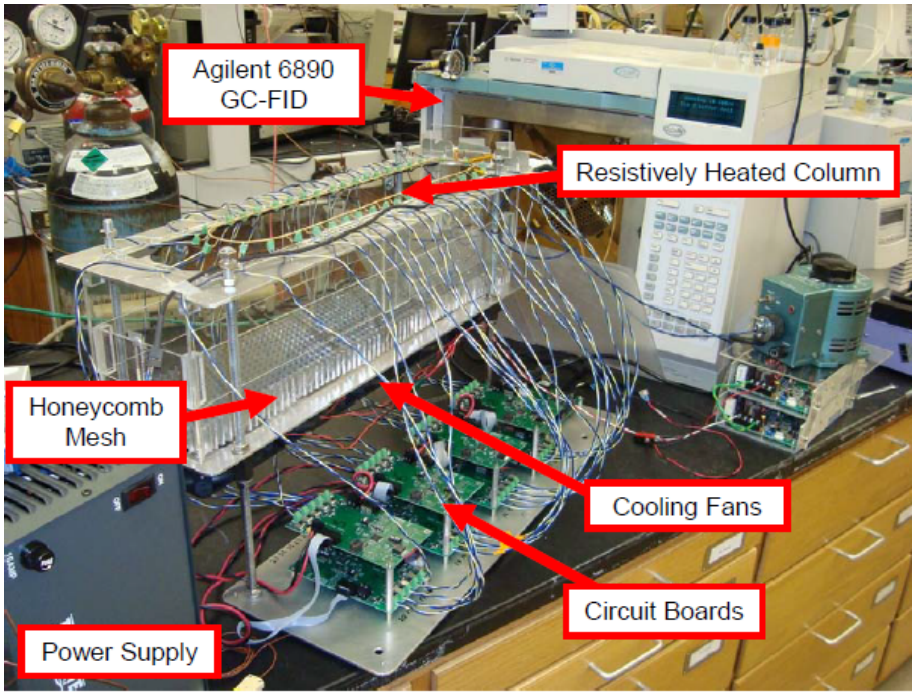

Figure 11: Laboratory setup for the moving TGGC system for the generation of flexible temperature gradients [16].

2.5.2 State-of-the-Art Instrumentation of NTGC

The research group of Boeker at the University of Bonn published and patented an innovative design for TGGC.[15, 27] Their setup consisted of a cylindrical tower with a helical structure engraved for housing the column which is directly and resistively heated by being kept inside of a stainless steal capillary. The inside of the cylinder is filled with a foam providing a controlled flow resistance. The temperature gradient is introduced by a fan cooling from the bottom up leading to the desired negative thermal gradient since the cooling effect at the end of the cylinder is the strongest. This system is connected to commercially available injection/detection units. The initial concept was presented in 2015 [15] while its applications was shown in [17] and [28]. This setup enables low elution temperatures, hyperfast measurements due to fast heating and cooling cycles while maintaining high reslution. [15] This instrument later became, as the first of its kind, commercially available and is shown, as a sketch, in Figure 12.

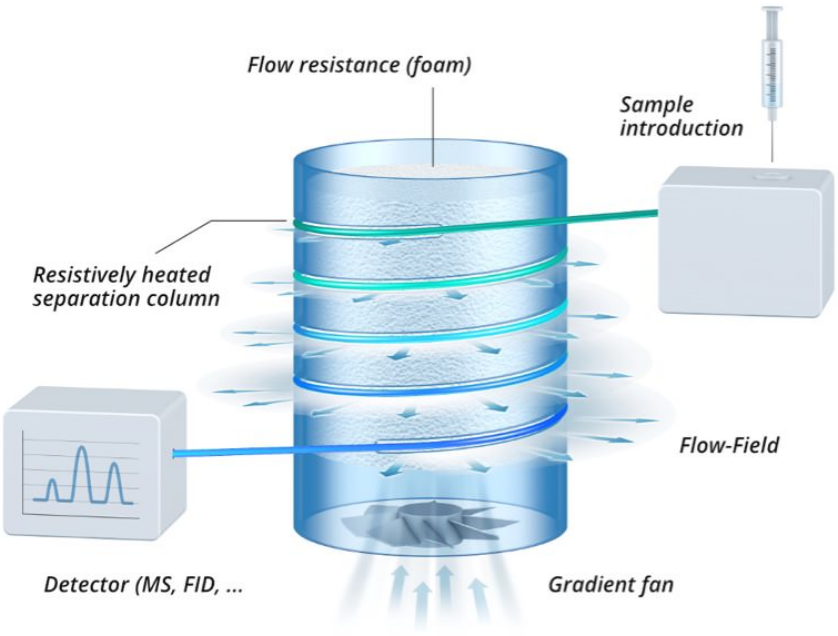

Figure 12: Sketch of the TGGC setup by Boeker et al. commercially at HyperChrom S.A. [29].

3 Setup and Electronic Control

The following chapter provides a concise summary of the various types of temperature measurement and control since these terminologies are crucial for following chapters 4, 6, 7 and 8

3.1 PID Controlling

PID control, short for proportional-integral-derivative, is one of the most common control methods in automation and control technology. It is a powerful tool used in a wide range of applications, from temperature control in household appliances to the control of industrial processes. [30, 31]

3.1.1 Principles of PID Controlling

PID control is based on the principle of regulating a variable temperature, speed or pressure (in this work PID controlling will only be responsible for temperature control) to a desired setpoint. The PID controller uses three main components:

Proportional (P): This part of the controller generates an output change that is proportional to the error between the setpoint and the actual value of the controlled variable. The greater the error, the greater the correction made by the P component of the controller. A high P-gain can lead to a fast response of the system, but also to an increased risk of overshoot and oscillation.

Integral (I): The I component of the controller takes into account the entire history of error values over time. It corrects slow, continuous errors that cannot be eliminated by the P component. This part of the controller prevents the system from permanently deviating from its setpoint.

Derivative (D): The D portion of the controller looks at the rate of change of the error. It helps to reduce overshoot and oscillation by responding to rapid changes in the error. The D part can contribute to enhancing the overall stability of the system.

The output signals of the P, I and D components are added together to produce the control signal that is used to adjust the system.[30, 32]

3.2 Temperature Measurements

In this work two different methods for temperature measurements have been used. Those will be briefly explained in the following sections.

3.2.1 NTC Resistors (Negative Temperature Coefficient Resistors)

NTC resistors are a special type of resistive element used in a variety of applications due to their unique electrical properties. The abbreviation "NTC" stands for "Negative Temperature Coefficient", which indicates that the electrical resistance of these components decreases with increasing temperature.

NTC resistors are made of semiconductor materials that are able to drastically alter their electrical resistance in response to changes in temperature. Unlike conventional resistors with a constant resistance value, NTC resistors are highly susceptible to thermal fluctuations, making them ideal for temperature measurement and compensation.[33, 34]

The resistance temperature characteristic of an NTC resistor is highly non-linear, meaning that the resistance does not decrease or increase at a constant rate, but rather exponentially as a function of temperature. This enables precise temperature measurements in the prescribed temperature range but drifting will occur at higher temperatures. The principle of operation of NTC resistors is based on the temperature dependence of the charge carrier concentration in the semiconductor material. As the temperature rises, the concentration of charge carriers and therefore the conductivity of the material increases. This leads to a decrease in the electrical resistance of the NTC resistor which is being used for precise temperature measurements.[33, 34]

3.2.2 Type K Thermocouples

Type K thermocouples, also known as Chromel-Alumel thermocouples, are one of the most common types of thermocouples used for temperature measurement and monitoring in various applications. The working principle of thermocouples is based on the Seebeck effect, which is a phenomenon where a voltage is generated when two dissimilar metals or conductors are joined together with different temperatures on both sides. This voltage is proportional to the temperature difference between the two junctions. Type K thermocouples are characterised by the following attributes: [33, 35]

- Temperature range: type K thermocouples can be used in a wide temperature range, from around -200 °C to +1350 °C (for short term use, for long term use up to 800 °C) This makes them ideal for applications with extreme temperatures.
- Robustness: These thermocouples are generally very robust and resistant to

mechanical stress. They can be used in the harshest environments.

- Fast response time: They respond quickly to temperature changes, which is an advantage in process control applications and laboratory environments. The voltage changes by 41 µV per °C which is given by the Seebeck coefficient.
- Low cost: Type K thermocouples are inexpensive to manufacture and purchase, making them economically attractive.

Due to these properties Type K thermocouples are often used in industrial process controlling and heating / cooling systems. In this work a special type of Type K thermocouple was used.[36] These were chosen due to their low thermal mass since their measurement head is only 0.076 mm in diameter. This was used in chapter 8.[33, 35]

4 Setup 1: Agilent 6890-N with FID

As a theoretical, instrumental and experimental base for the construction of the here presented setup Boeker et al.'s [15] design for the field flow thermal gradient GC (FF-TGGC) was utilized (see section 2.5.2). The ideas presented in [15] were adapted and put into the design of the TGGC module, from now on referred to as "cooling tower", by Mueller [2]. The following section will focus on the construction of the module, achieved results of the module and also show a comparison between TGGC and fast gas chromatography (directly heated steel capillary for fast heating rates and faster elution, but no spatial thermal gradient implemented). For a more detailed description of the setup construction the reader is invited to read the Master thesis of Mueller [2].

4.1 Instrument

The instrument the cooling tower was connected to was an Agilent 6890-N (Agilent Technologies (Santa Clara, California, USA) gas chromatograph equipped with a FID. The gas chromatograph was used as an injection unit using its autosampler, as flow regulator using its EPC (electronic pneumatic control) and as detection unit. The FID is based on the principle of combustion and ionization. The eluting analyte is introduced to the detector and combusted in a hydrogen-air flame. In the flame combustion (= oxidation to CO_2) occurs. In this process carbon-carbon bonds of the analytes are broken forming positively charged ions (carbenium-ions) and electrons. These electrons are responsible for a current that can be measured. The intensity of the detected current is proportional to the number of carbenium ions formed and therefore proportional to the concentration of the compound reaching the detector.[10].

4.2 Cooling Tower

4.2.1 Heating of the Steel Capillary

The capillary column itself was kept inside of a stainless steel capillary similar to the one shown in [15] with the main difference being that the capillary in this setup was 1.5 meters long. The capillary was acquired from SWS Edelstahl GmbH & Co. KG, Emmingen-Liptingen, Germany and was made out of 1.4301 stainless steel. The outer diameter was 1.0 mm with a wall thicknesss of 0.1 mm and it had a resistance of 5 Ω. The steel capillary was resistively heated using a power supply with a maximum voltage of 30 V, maximum current of 10 A resulting in a

maximum power of 300 W. Temperature measurements have been performed using Type K thermocouples which where connected to the stainless steel capillary using thermal paste and kapton tape (to prevent short circuits). The temperature was controlled by PID controlling. The system itself was controlled by two Arduino's using the code in the appendix with the Arduino IDE [37]. The circuit diagram for controlling the cooling tower is presented in Figure 59 in the appendix.

4.2.2 Transferline Heating

The introduction of transferlines was necessary to keep the capillary column hot while also directly connecting them to the injection and detection unit of the gas chromatograph. The transferlines were heated by leading the capillary column through a resistively heated coiled wire. The wire was made of a CuNi44 alloy with a diameter of 0.6 mm and a specific electrical resistance of 0.49 $(\Omega mm^2)/m$. Its power was PID controlled by the circuit (Figure 59) and code shown in the appendix. It is important to note that only the part of the capillary column wrapped around the cooling tower was inside the stainless steel capillary. Both transferlines were then sleeved with a fiber glass tube for thermal insulation. A picture of the transferline is shown in Figure 13.

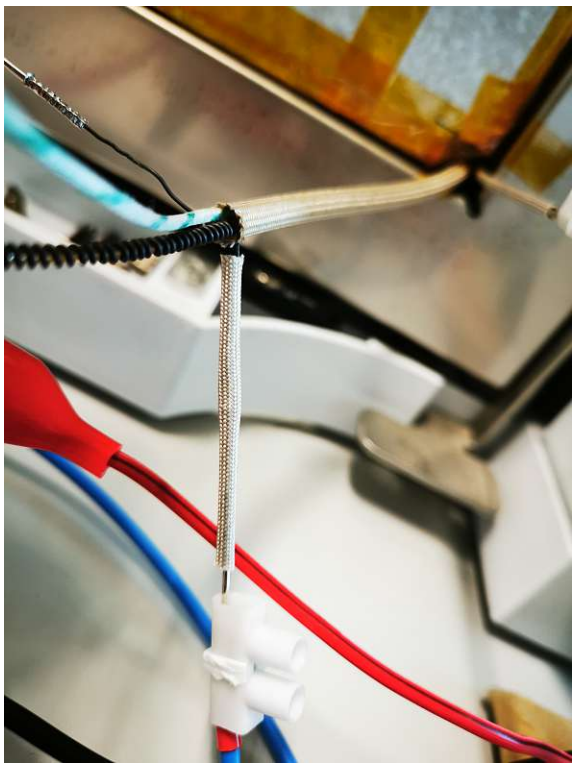

Figure 13: Close up of the transferline for the cooling tower setup.

4.2.3 Cooling System

Figure 14 (right) depicts the cooling system of the cooling tower. The hull itself was 3D printed and consists of an acrylonitrile butadiene styrene copolymer. It is 20 cm in height and its outer diameter spans a width of 10 cm resulting in a circumference of approximately 31.4 cm. Additionally, as can be seen in Figure 14 right, the hull is mounted on a pedestal enabling the connection to the fan by which the temperature gradient is created. As a filling material for controlling the airflow inside of the hull a commercially available aquarium filter material was used. This material was chosen after a trial and error approach of testing airflow resistances in [2].

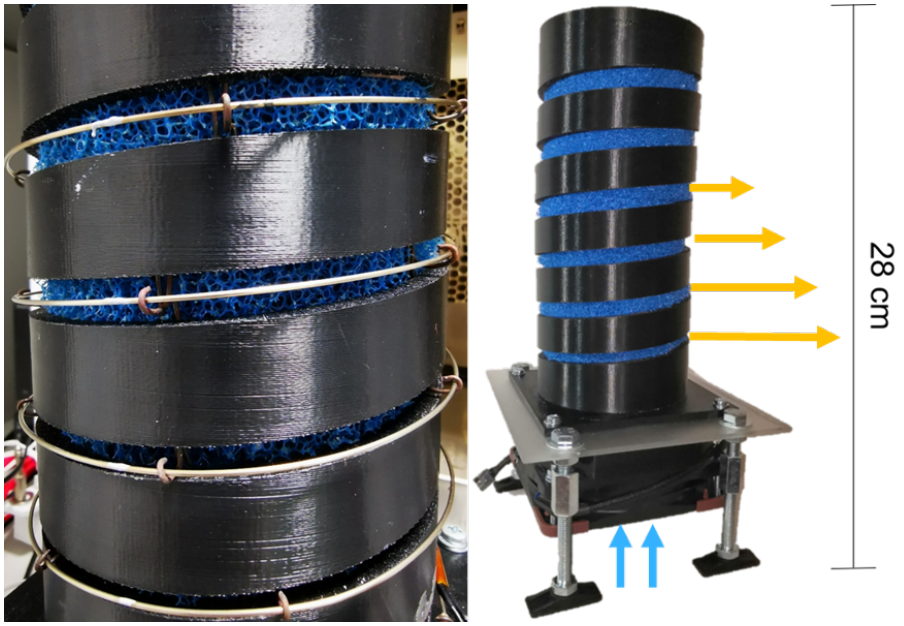

Figure 14: Left: Close up of the hull housing the steel capillary. Right: Depiction of the cooling system, with the fan cooling from underneath (blue arrows) resulting in a larger removal of heat at the bottom (yellow arrows).

As a fan a 12 V DC, NF-F12 industrial PPC-3000 PWM fan with a diameter of 12 cm by "Noctua" (Rascom Computerdistribution, Vienna, Austria) with a maximum airflow of 186.7 m^3/h was used. For controlling its revolutions per minute its 4-pin connection was installed allowing pulse width modulation (PWM) for regulating cooling power. Lastly, as can be seen in Figure 14 on the left the column inside of the steel capillary had to be held close to the airflow and therefore to the hull. To realize that, clamps made from iron wire were used and loops were formed which were capable of holding the steel capillary.

4.3 Using the Cooling Tower with the Instrument

After construction of the cooling tower it had to be connected to the gas chromatograph. This was achieved by connecting the capillary column (Supelco SLB-5MS, 2.5 m x 0.1 mm x 0.1 µm) to the injection and detection unit of an Agilent 6890-N. The connection, or rather a picture of the whole setup setup is illustrated in Figure 15. The oven of the gas chromatograph itself was used to keep a constant temperature of ∼200 °C and was later closed with a cover since the original door could no longer be closed due to the transferlines reaching into the system.

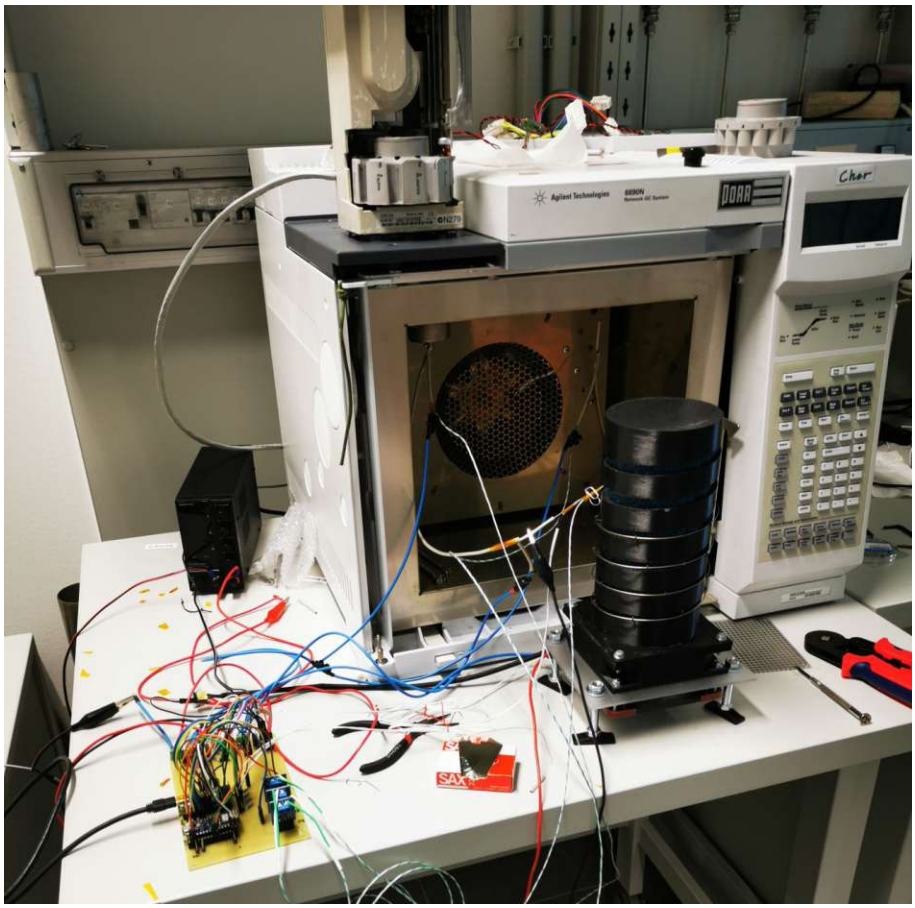

Figure 15: Photograph taken of the TGGC-FID setup.

4.3.1 Measurements of the n-Alkane Standard

Many measurements with this setup have been performed even before the begin of this thesis. The outcome of the optimization approaches have been presented by Klampfl et al. [14] in form of a conference poster. With this setup high heating rates (up to 1000 K/min and even higher) were achievable. A standard containing n-C_8 to n-C_{20} standard in n-hexane with a concentration of 40 mg/l by *Supelco*^{TM}(Merck, Darmstadt, Germany, EC-Nr.: 04070-5 ml) was used to characterize and evaluate

Table 2: Measurement parameters for the measurement of the n-octane - n-eicosane standard shown in Figure 16.

Parameter	Value
Injection volume / µl	1
Injector temperature / °C	250
Split	150:1
Transferline temperature / °C	160
He flow / ml min^{-1}	0.5

the system. In Figure 16 both are shown: on the one hand the heating ramp, representing the temperature gradient between the TGGC inlet and outlet and on the other hand, the resulting chromatogram. The measurement paramaters of the measurement are summarized in Table 2. The results were remarkable with n-octane to n-eicosane eluting in a time span of only twelve seconds all of which additionally showing baseline separation.

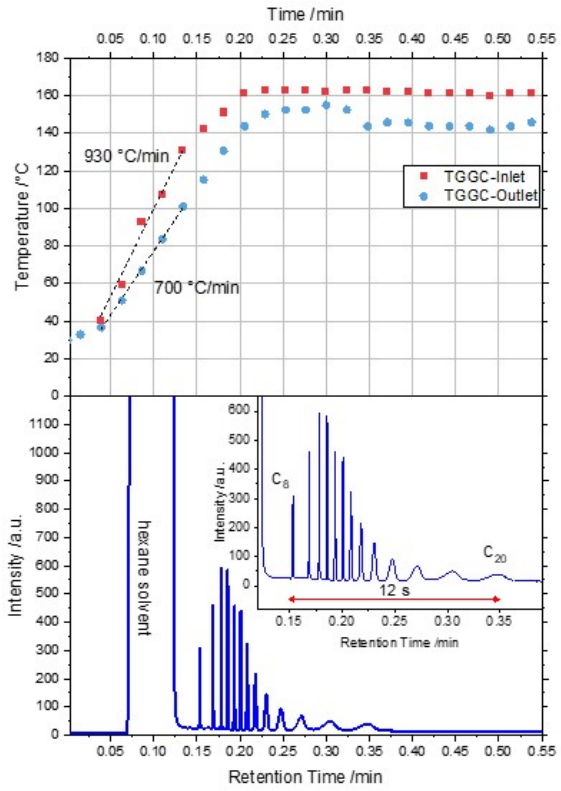

Figure 16: Top: Heating curves for inlet and outlet of the TGGC for the chromatogram shown in the bottom. Bottom: Chromatogram acquired with the TGGC-FID setup with a cutout of the twelve second elution interval of n-C_8 to n-C_{20}.

4.3.2 Comparison to a Reference Measurement with a Fast GC

In order to demonstrate that a negative thermal gradient in TGGC has an advantage over fast gas chromatography without a thermal gradient, a reference measurement with a self built fast GC was performed. Both significantly shortened measurement times due to the short column lengths while drastically losing in capacity. The remaining factor of the "optimization triangle" (Figure 17) being able to distinguish between the two setups is the high resolution which is claimed to be achieved by introducing the negative thermal gradient.

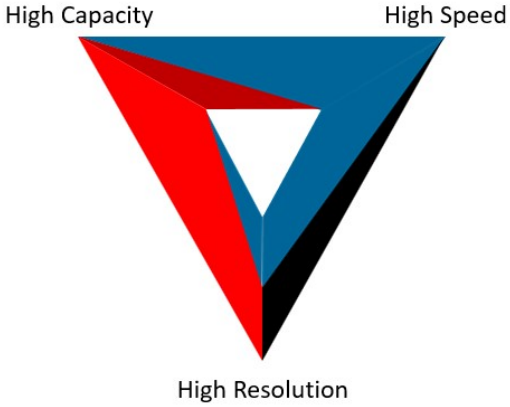

Figure 17: Optimization triangle after [38].

The main difference between the fast GC and the TGGC-FID is that no negative thermal gradient is implemented in fast GC. Both of the setups were resistively heated using a steel capillary enabling high heating rates and fast elution. The reference measurement was performed using the same column length as in the cooling tower setup and put into a steel capillary. The capillary was then directly connected to the injection/detection unit of a *Shimadzu*^{TM} *FID-2010 Plus* gas chromatograph. The heating was controlled by using the same power supply used with the cooling tower.

The results of the fast GC measurement (Figure 19) are compared with the TGGC measurement (Figure 18). From the Figures it is evident that the shorter retention times stem from the column length since both chromatograms are approximately acquired within more or less same amount of time (with TGGC being one minute faster). The biggest discreprancy between the two chromatograms is the difference in resolution. While all peaks are completely baseline separated for the measurement with the TGGC-FID setup, this is not the case for the measurement using the fast GC without negative thermal gradient. So it was proven that peak focusing effects of

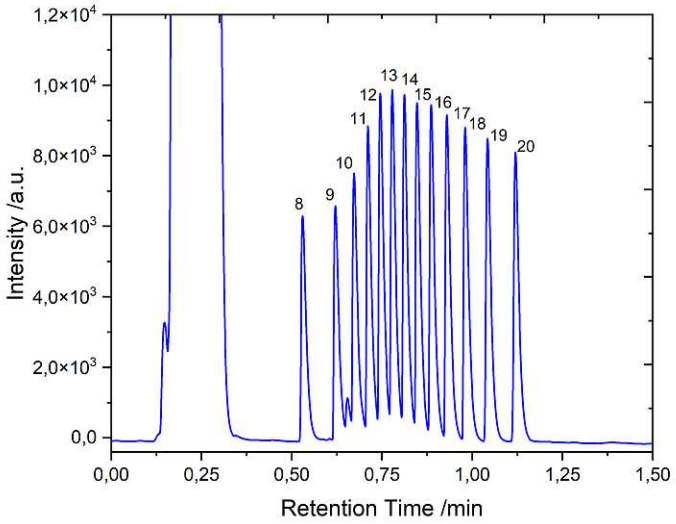

Figure 19: Chromatogram acquired with the Fast GC for comparison with the TGGC-FID setup.

the negative thermal gradient had a positive influence on the chromatographic performance of the system whilst maintaining and even enhancing fast elution speeds.

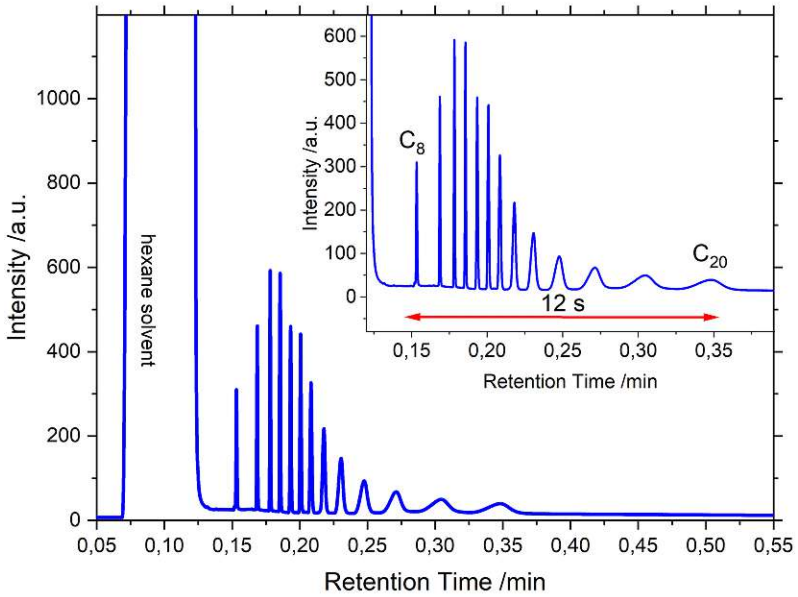

Figure 18: Chromatogram acquired with the conditions shown in Table 2.

5 Simulation of Cooling Tower NTGC setup

5.1 Isothermal Measurements on GC-FID

To acquire data to calculate the thermodynamical parameters necessary to create a database for the simulation isothermal measurements of a n-C_8 - n-C_{20} standard in n-hexane with a concentration of 40 mg/l by *Supelco*^{TM}(Merck, Darmstadt, Germany, 04070-5 ml) have been conducted similar to Karolat et al. [39]. The measurements were performed on a *Shimadzu*^{TM} *FID-2010 Plus* gas chromatograph by Shimadzu (Duisburg, Germany) equipped with two FIDs of which one was used. A *Restek*^{TM} *Rtx*^{TM}*-5MS* column was used whose specifications are displayed in Table 3. The temperature range in which the experiment was done was 50-220 °C. The remaining parameters are shown in Table 4. All measurements were executed in constant linear velocity mode. The chromatograms were evaluated using *Shimadzu*^{TM} *LabSolutions*^{TM} software. As an example the chromatogram for the isothermal measurement at 180 °C is reported in Figure 20.

Table 3: Column specifications of Rtx^{TM}-5MS column.

Column Specifications	
Name	Rtx-5MS Low-Bleed-GC Capillary Columns
Length / m	30
d_f / µm	0.25
Inner diameter / mm	0.25
Temperature range / °C	-60 to 330
Stationary phase	5% Diphenyl/95% Dimethylpolysiloxane

Table 4: Chromatographic Parameters for Isothermal Measurements.

Measurement Parameters	
Injection temperature / °C	250
FID temperature / °C	300
Carrier gas	Helium
Linear velocity / cm s^{-1}	27.6
Injection volume / µl	1
Isothermal temperatures / °C	50 - 220 (in steps of 10 °C)
He flow / ml min^{-1}	1
Split ratio	1:50

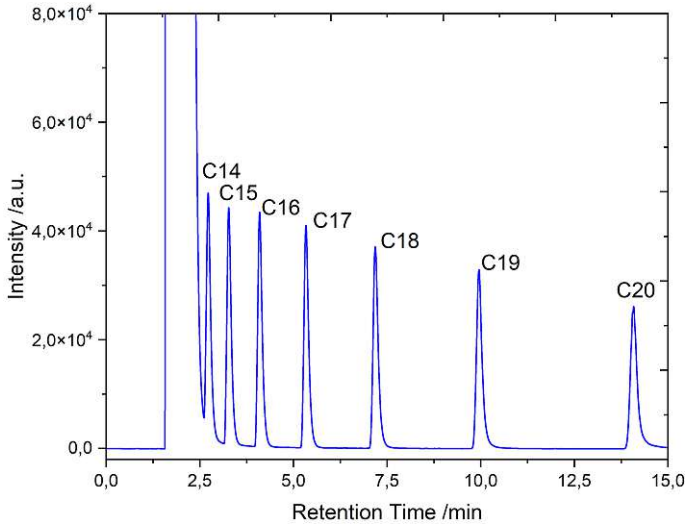

Figure 20: Exemplary chromatogram for isothermal measurement at 180 °C.

5.2 Calculation of Dead Time

The determination of dead time in gas chromatography can be conducted in many different ways. For example using an mass spectrometric detector one could assign the retention time of air as dead time whilst co-injecting methane is also an option. In this work different methods of dead time calculation were tried. Firstly the approaches by Peterson and Hirsch [40] were applied. Their method based on relating a peak to an arbitrarily chosen point instead of the real dead time. Using three representatives of the homologous series the distance from the chosen point to the dead time can be calculated and respectively the dead time. [41]

Still the method shown in Quintanilla-Lopez et. al [42] and Wu et. al [43] yielded the best results. It included plotting t_r against the number of carbon atoms and performing a four parameter fit shown in equation 1, where t_r is the retention time in minutes, z is the number of carbon atoms and A, B, C and D are the parameters. For calculation of the dead time, the curve was extrapolated to $z = 0$, meaning zero carbon atoms. A plot of the fit for a temperature for 180°C is shown in Figure 21. The fits were performed for every temperature in the range of the isothermal measurements (50-220°C).

$$t_r = A + e^{(B+Cz^D)} \tag{1}$$

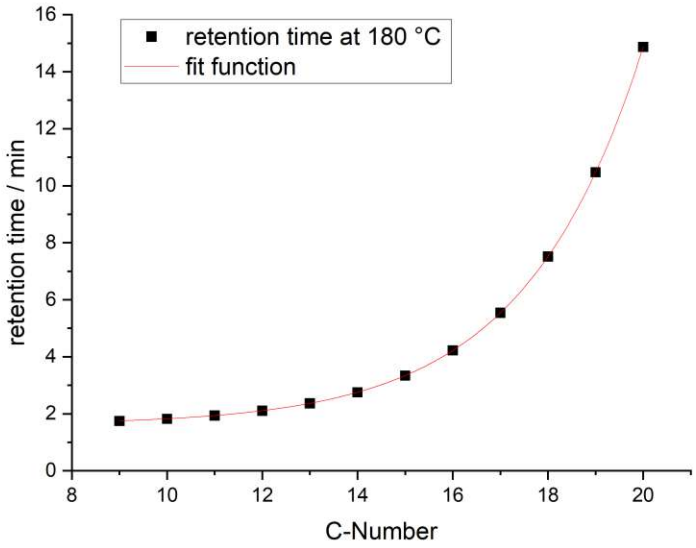

Figure 21: Four parameter fit for a temperature of 180 °C.

5.3 Calculation of Thermodynamical Data

To calculate the necessary parameters for the simulation one has to determine the retention factor (k) at each temperature which results from equation 2, with the retention time of the analyte (t_a) and retention time of an unretained species (t_s). Consequently the partition coefficient (K) can be determined by equation 3 with the concentration of the analyte in the stationary phase (c_s), the concentration of the analyte in the mobile phase c_m and the phase ratio (β). βitself can be approximated via equation 4 using the inner column radius r_i and the film thickness d_f.[39]

$$k = \frac{t_a - ts}{t_s} \tag{2}$$

$$K = \frac{c_s}{c_m} = k\beta \tag{3}$$

$$\beta \approx \frac{r_i}{2d_f} \tag{4}$$

To accurately determine thermodynamic parameters, it is essential to take into account the temperature-dependent nature of the partition coefficient which was realized by doing a three-parameter fit of the natural logarithm of K, the inverse temperature and the natural logarithm of the temperature shown in equation 5. The fit was performed using SciPy optimize curve fit. As an example, Figure 22 shows

the plot of the three-parameter-fit for n-tetradecane.

$$ln(K) = A + B\frac{1}{T} + Cln(T) \tag{5}$$

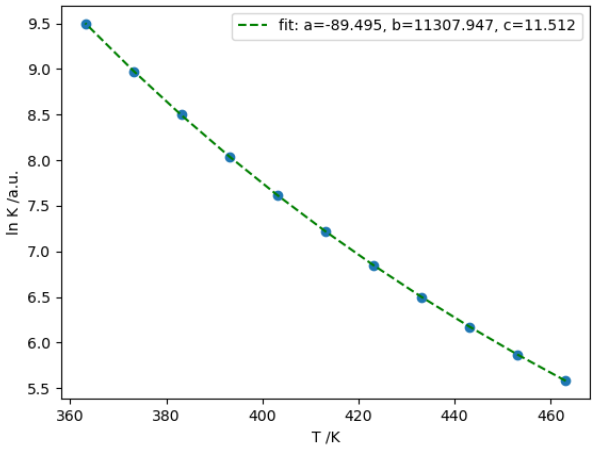

Figure 22: Three-parameter-fit for n-tetradecane (a,b,c resemble the fit parameters A,B,C).

According to [39],[44], [45] and [46] the three parameters can be described as shown in the following equations 6, 7, 8 where R stands for the ideal gas constant, $\Delta H(T_0)$ describes the enthalpic change at a chosen reference temperature and $\Delta S(T_0)$ is the change in entropy respectively. The chosen reference temperature in Karolat et al. [39] was 90 °C. The isobaric molar heat capacity (ΔC_p) can then be calculated from parameter C.

$$A = \frac{\Delta S(T_0) - \Delta C_p ln(T_0) - \Delta C_p}{R} \tag{6}$$

$$B = -\frac{\Delta H(T_0) - \Delta C_p T_0}{R} \tag{7}$$

$$C = \frac{\Delta C_p}{R} \tag{8}$$

Additionally, when not taking into consideration the temperature dependence of ΔC_p (as shown in [47], [48]) and neglecting the temperature dependent enthalpical and entropical changes correlated to the transition of analytes between stationary and mobile phase and in vicinity of the reference temperature $T = T_0$, A and B can be simplified to equations 9 and 10, resembling the form of A and B from a two-parameter-fit shown in Karolat et al. [39, 44, 49]

$$A = \frac{\Delta S}{R} \tag{9}$$

$$B = -\frac{\Delta H}{R} \tag{10}$$

After having calculated the three model parameters for all analytes the thermodynamical values relevant for the database for the simulation were computed via the approach shown by Blumberg in 2017.[49] The parameters T_{char} (equation 11) and θ_{char} (equation 12) correspond to the values of T and θ at k = 1. θ itself is a thermal constant describing the change in k and K with respect to the temperature.

$$T_{\text{char}} = \frac{\Delta H}{\Delta S - Rln(\beta)} \tag{11}$$

$$\theta_{char} = \frac{-RT^2{}_{\text{char}}}{\Delta H} \tag{12}$$

5.4 Resulting Thermodynamical Values

The fit parameters A, B and C are illustrated in Figure 23. The database, being a summary of thermodynamical values for all analytes, CAS-numbers, categories and columns can be found in Table 5.

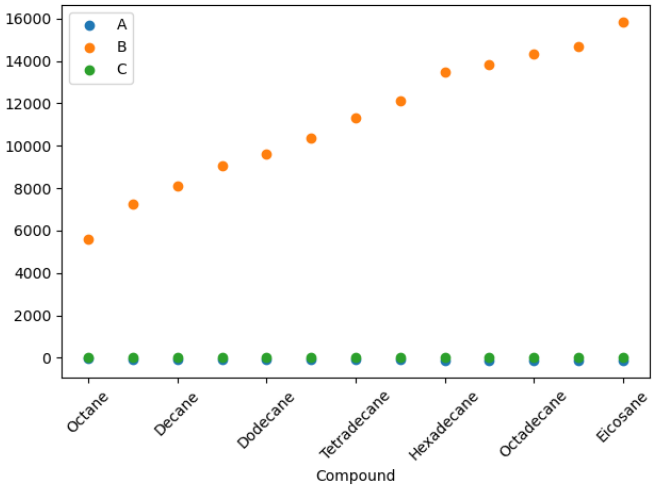

Figure 23: Plot of the parameters A,B and C for all components analyzed.

Table 5: Summary of CAS numbers, stationary phases and thermodynamical values for all analytes based on experimental data.

Name	CAS	Phase	T_{Char}/K	Θ_{char}/-	ΔC_p/JK^{-1}mole^{-1}	φ_0	Category
Octane	111-65-9	Rtx-5MS	65.97	27.28	33.93	0.001	Alkanes
Nonane	111-84-2	Rtx-5MS	86.55	27.97	60.44	0.001	Alkanes
Decane	124-18-5	Rtx-5MS	105.43	28.92	68.76	0.001	Alkanes
Undecane	1120-21-4	Rtx-5MS	122.86	29.35	78.59	0.001	Alkanes
Dodecane	112-40-3	Rtx-5MS	139.30	30.17	80.37	0.001	Alkanes
Tridecane	629-50-5	Rtx-5MS	154.41	30.57	86.54	0.001	Alkanes
Tetradecane	629-59-4	Rtx-5MS	168.68	31.45	95.71	0.001	Alkanes
Pentadecane	629-62-9	Rtx-5MS	182.11	31.77	102.33	0.001	Alkanes
Hexadecane	544-76-3	Rtx-5MS	194.92	32.28	120.21	0.001	Alkanes
Heptadecane	629-78-7	Rtx-5MS	206.62	31.82	117.86	0.001	Alkanes
Octadecane	593-45-3	Rtx-5MS	217.48	31.38	119.81	0.001	Alkanes
Nonadecane	629-92-5	Rtx-5MS	227.53	30.90	118.17	0.001	Alkanes
Eicosane	112-95-8	Rtx-5MS	237.09	30.58	131.50	0.001	Alkanes

5.5 Simulating Chromatograms Using Lepperts Julia Script

After providing the script with the correct measurement parameters (flow, temperature gradient, column size,...) the chromatograms for our system were simulated by Leppert's GasChromatographySimulator.jl[50]. In Figures 26 to 25 the resulting chromatograms for maximum cooling tower temperatures of 180°C, 220°C and 250°C are displayed. For comparison a measurement acquired with Setup 1 (section 4) is depicted in Figure 27.

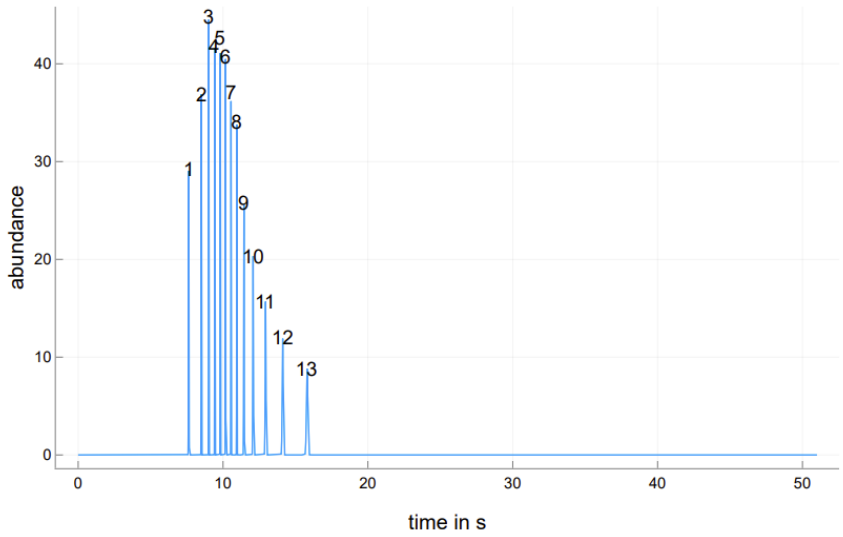

Figure 24: Simulated chromatogram for a final run temperature of 220 °C. The peak assignments 1-13 correspond to C_8 to C_{20} n-alkanes.

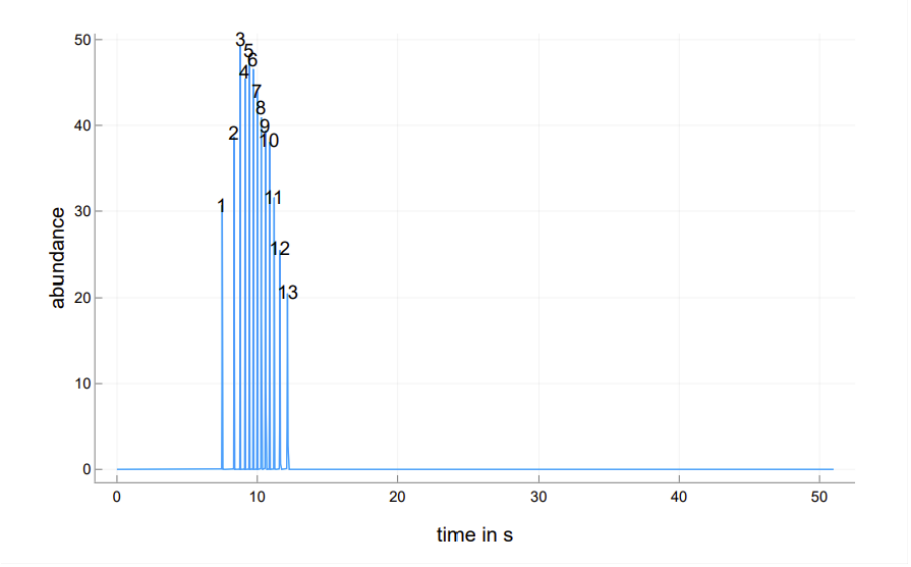

Figure 25: Simulated chromatogram for a final temperature of 250 °C. The peak assignments 1-13 correspond to C_8 to C_{20} n-alkanes.

5.6 Conclusions Drawn from the Simulation

5.6.1 Diffusion of Volatile Compounds at Room Temperature

Comparing Figures 26 and 27 where the experimental heating ramp and the simulated heating ramp are the same one can see that the peak pattern (related to the spacing and intensity of the peaks) in the two chromatograms is almost the same meaning that the experimental results are at least partly backed by theory. For both chromatograms n-octane and n-nonane showed lower intensities than some of their successors in the homologous series of n-alkanes which is quite surprising since they should show less interactions with the stationary phase at higher temperatures which should lead to less peak broadening and therefore undiminished height (taking into consideration that all of the peaks should have the same area due to all compounds having the same concentration in the sample). The same trend applies also to the simulated chromatograms at higher temperatures in Figures 24 and 25. Additionally, for all chromatograms the peak of n-octane is separated from the following peaks by a larger interval than for the subsequent peaks.

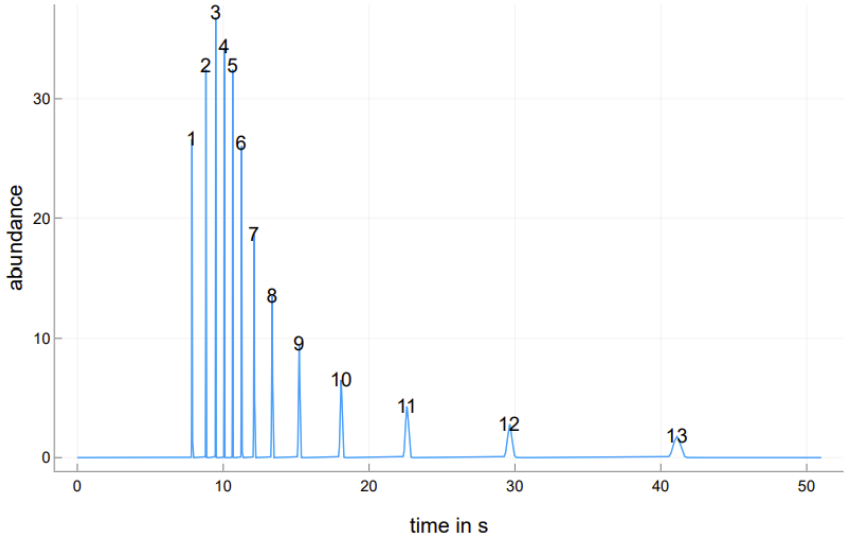

Figure 26: Simulated chromatogram for a final temperature of 180 °C. The peak assignments 1-13 correspond to C_8 to C_{20} n-alkanes.

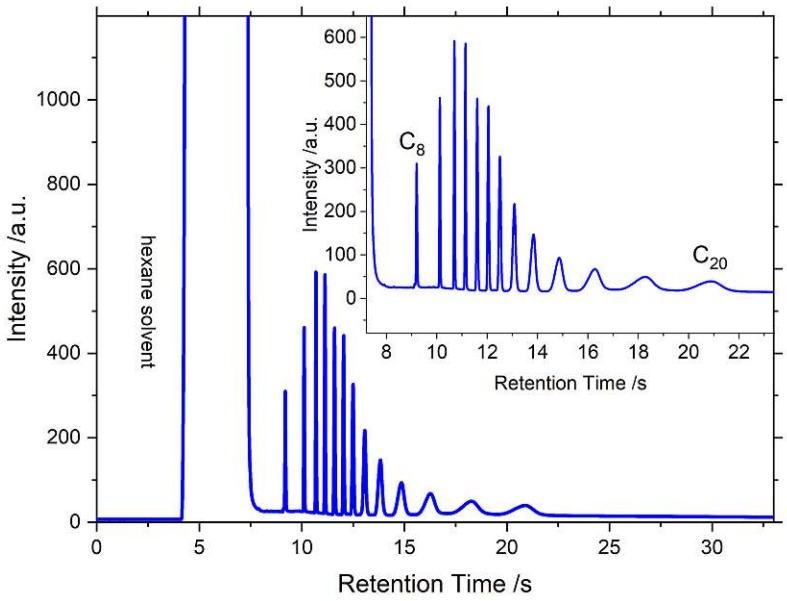

Figure 27: Experimental chromatogram acquired with cooling tower setup 1 (chapter 4), final run temperature 180 °C for comparison with the simulation (figure 26).

This phenomenon is explainable looking at the plots shown in Figures 28 to 30. These represent the relationship between the position of the analyte along the column and the time in seconds. Each of the curves represent one of the analytes of the homologous series, starting with octane from left to right. By taking a closer look at these plots it is evident that almost all analytes remain parked at position

z = 0 until a time t of approximately five to six seconds. This results from the fact that a five second delay between measurement start and start of the heating ramp is implemented into the code controlling the cooling tower or in this case implemented into the heating ramp of the simulated measurement. n-octane, n-nonane and partly n-decane are deviating from the behaviour of the other analytes. Looking at the curves for those three it can be seen that these analytes start moving through the column even before the start of the heating ramp meaning that their interaction with the stationary phase is insufficient to retain the analytes at the beginning of the column before initiating the heating ramp. Since the retention is still increased for n-octane, n-nonane and n-decane at room temperature peak broadening occurs counteracting the peak focusing effect achievable by using negative thermal gradient gas chromatography. The broadening occurs strongest for n-octane due to it travelling the fastest and furthest at room temperature.

Gaining this insight by the z over t-plots explains the peak pattern and also the larger intervals between the most volatile n-alkanes (n-octane, n-nonane and n-decane) in the chromatograms in Figures 24, 25 and 26. This also means that results of the measurements performed are highly dependent on environmental conditions in the laboratory since the migration of n-octane, n-nonane and n-decane varies with room temperature. As a result, for performing reproducible measurements with any of the setups shown in chapters 4 to 8 a constant laboratory temperature should be kept and the setup itself should be shielded from air circulation to prevent temperature fluctuations. Additionally, for achieving the narrowest possible injection bands and reducing diffusion at room temperature the whole setup could be cooled below room temperature by tempering the airflow to the casing of the setup. This should allow parking of all analytes at the beginning of the column resulting in even narrower peaks and more reproducible results.

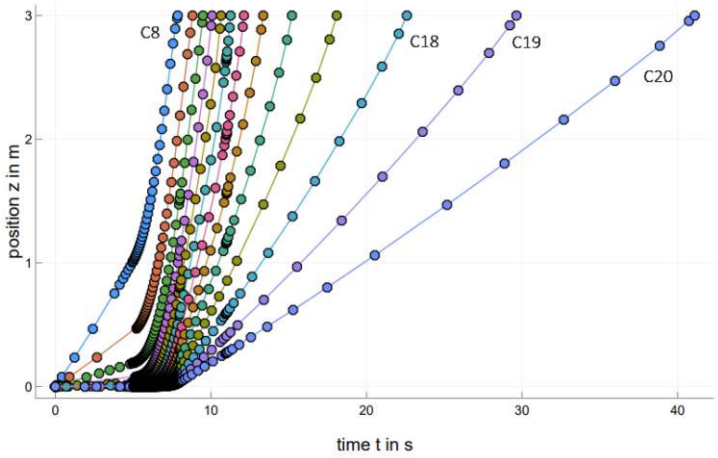

Figure 28: Simulated analyte postions along the column (z) plotted against time in seconds for chromatogram shown in Figure 26. Each of the curves represents one analyte from n-octane to n-eicosane, starting with n-octane from left to right. Conditions shown in corresponding chromatogram.

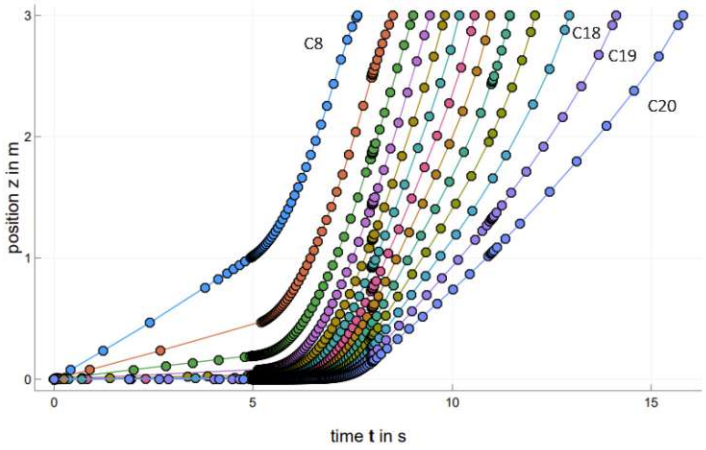

Figure 29: Simulated analyte postions along the column (z) plotted against time in seconds for chromatogram shown in Figure 24. Each of the curves represents one analyte from n-octane to n-eicosane, starting with n-octane from left to right. Conditions shown in corresponding chromatogram.

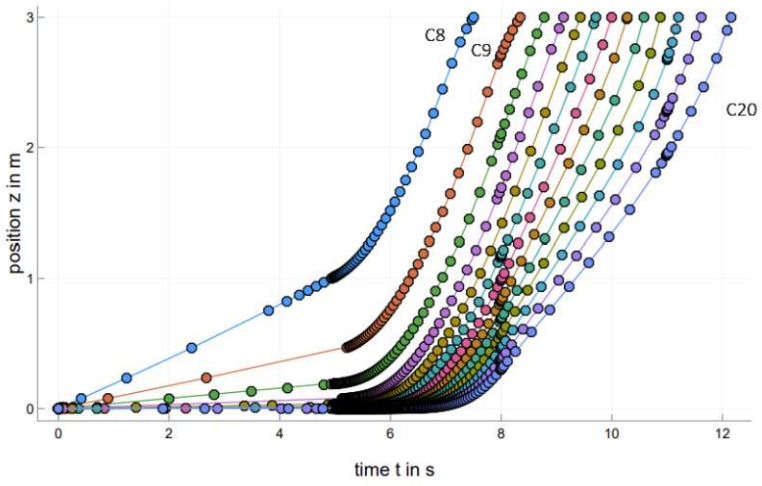

Figure 30: Simulated analyte postions along the column (z) plotted against time in seconds for chromatogram shown in Figure 25. Each of the curves represents one analyte from n-octane to n-eicosane, starting with n-octane from left to right. Conditions shown in corresponding chromatogram.

5.6.2 Peak Broadening

Looking at Figures 26 and 27 it is evident that the peak broadening in the experimental chromatogram is worse than in the simulation. This most likely results from the simulation taking ideal heating curves into account. These ideal heating curves were experimentally not achievable due to latency in heating and also to some inaccuracies in temperature measurements. Additionally, this may be caused by yet undiscovered coldspots in the setup or non ideal sample transfer.

5.6.3 Shorter Retention Times in Experiment

As a last difference between the simulated chromatogram (Figure 26) and the experimental chromatogram (Figure 27) the shorter retention times in the experiment have to be mentioned. While n-eicosane elutes at ∼42 seconds in the simulation it elutes at ∼33 seconds in the experiment. This can be reasoned by the simulation applying the negative thermal gradient to the whole three meters of column length. In the experimental setup (shown in chapter 4) only 1.5 meters of the column are actually inside the cooling tower and thereby affected by the negative thermal gradient. The remaining 1.5 meters are used as the transferlines between the injection unit and the cooling tower or the between the detection unit and the cooling tower. These are usually held at a constant higher temperature than the maximum run temperature of the cooling tower leading to faster eluting peaks compared to the simulation.

6 Setup 2: Agilent 6890-N with DSQII-MS

After showing the capabilities of setup 1 it was time to adapt the cooling tower for the use desired in the OPERION project. As a first step a connection to a mass spectrometric detector had to be established to test the cooling towers compatibility with the same kind of detector used for in-situ LIB testing at the AIT.

6.1 Working Principle of a Quadrupole Mass Analyzer

The functioning principle of a quadrupole mass analyzer, commonly used in mass spectrometry, is based on the application of both electric and radio frequency (RF) oscillating fields to selectively filter and separate ions based on their mass-to-charge ratio (m/z). [8, 51]

A quadrupole mass analyzer consists of four parallel metal rods arranged in a square or rectangular configuration, serving as electrodes. Direct current (DC) and radio frequency (RF) voltages are applied to these rods. The DC voltage creates a stable, static electric field, while the RF voltage generates an oscillating electric field.[8, 51]

Ions from the ion source (in this case electron impact ionization, short: EI, was utilized) enter the quadrupole. Depending on their m/z values, ions experience stable trajectories and pass through the quadrupole while all other ions are unstable and are deflected. Ions with the desired m/z values follow stable paths through the quadrupole, while ions with different m/z values are expelled from the path meaning that the quadrupole is sequentially scanning through the desired mass range. The user is also able to pre-select certain mass-to-charge ratios which are then exclusively measured during one measurement cycle, while not using measurement time for irrelevant signals, thereby improving the detection limits. This mode is called and referred to as selected (in case of more chosen m/z values) or single (in case of one chosen m/z values) ion monitoring mode (SIM).[8, 51]

After passing through the quadrupole, the selected ions are detected by a detector. Here a photo electron multiplier (PEM) was used. As a result a mass spectrum is acquired for every point in the chromatogram providing us with three dimensional information: the retention time, the intensity/abundance and the m/z ratio.

6.2 Interfacing the Cooling Tower with the GC and MS

In order to prepare the cooling tower for the connection with a system utilizing a mass spectrometic detection unit it was interfaced with a Thermo DSQII quadrupole mass spectrometer by Thermo Fisher Scientific (Waltham, Massachusetts, USA).

Additionally, an Agilent 6890-N gas chromatograph by Agilent Technologies (Santa Clara, California, USA) was used for gas flow regulation and as injector (Figure **??**). The respective ends of the capillary column reaching out of the cooling tower were connected to the injector and detection unit. The resulting setup is shown in Figure 31 with the Thermo DSQII on the left (together with the controlling computer), the cooling tower in the middle and the gas chromatograph on the right.[8, 51]

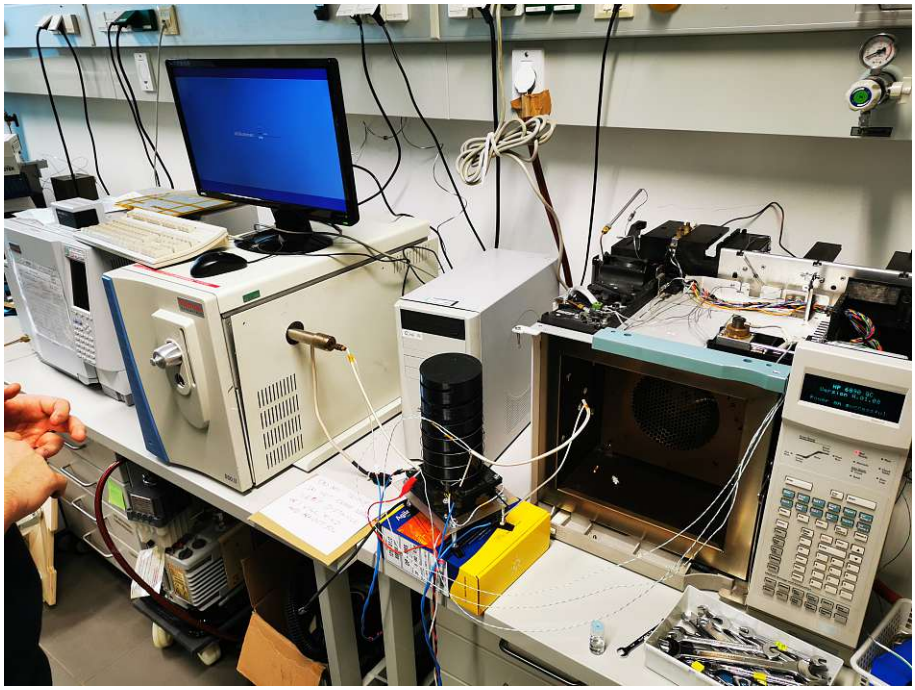

Figure 31: Cooling tower setup for use with the Thermo DSQII-Quadrupole mass spectrometer (left) coupled to the cooling tower (center) with the gas chromatograph for gas flow regulation and injection unit (right).

6.2.1 Transferline Heating of the DSQII

For the transferline of the injection side of the cooling tower no changes occured in this setup. Different to Setup 1 (section 4) the oven of the gas chromatograph could not be used for heating the remaining part of the capillary column - not resistively heated by a spiraled nickel wire - going to the detector (see Figure 31). To eliminate any possible cold spots resulting from the missing heating a solution had to be found. The mass spectrometer itself possessed a plug for connecting the transferline heating (=transfer from the end of the column to the ion source) to a suitable Thermo GC which was able to power the transferline heating. Unfortunately, no fitting connection could be established. As an alternative it was considered to wrap the whole transferline with heating wire. The same heating wire used for the transferlines shown in setup 1 (chapter 4) was wrung around the transferline of the mass

spectrometer. The process of installing the transferline heating is depicted in Figure 32.

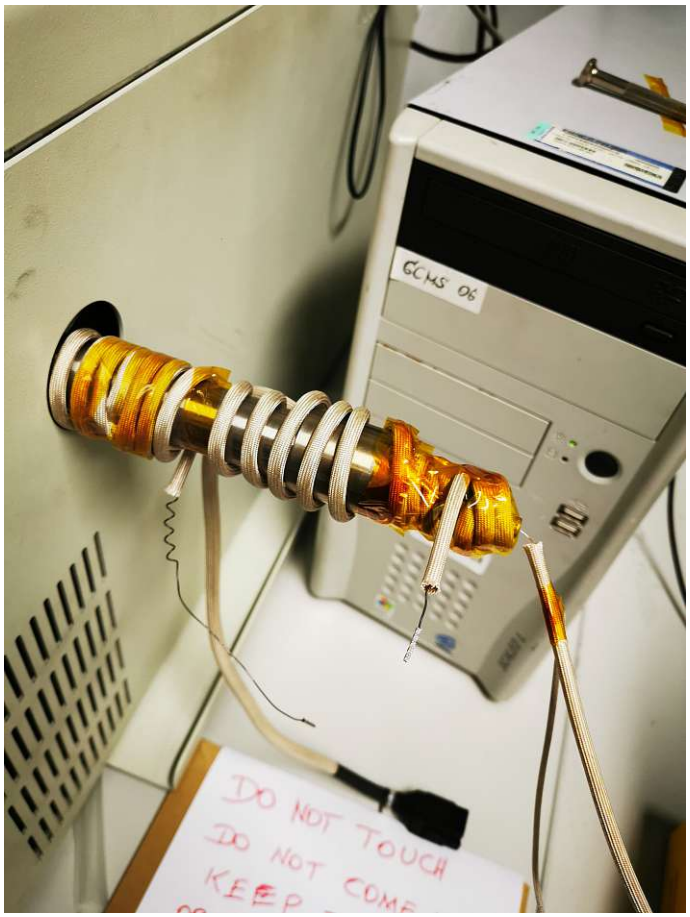

Figure 32: Construction of the transferline heating for the Thermo DSQII mass spectrometer.

After having tightly wrapped the whole transferline it was fixated using again a layer of Kapton tape. As can be seen in Figure 32 the column had to be handled with extreme care between the end of the transferline heating of the cooling tower (right) and the transferline of the MS (left) since mechanical stress would definitely lead to breaking the column. The transferline heating itself was powered by an external power supply with which current and voltage were adapted in order to achieve the desired temperature. For temperature measurements of the transferline, a NTC-resistor was fitted between the spiraled heating wire.

6.3 Implementation of a "Plug-And-Play" Concept

As evident from Figure 15 setting up the cooling tower as presented in chapter 4 is far from trivial and user friendly. Apart from dangers and health hazards coming

from non insulated wires and parts of the heating system, the whole setup was fragile and confusing. To adapt the instrument for routine use a simplification in its peripherals had to be performed.

The idea arose to house all of the electronics for controlling the cooling tower and the power supply in a box that can easily be transported and that the user would only have to plug all of the cables leading to the cooling tower in and is instantly ready to perform measurements.

For this purpose a grey plastic box ∼50x30x10 cm in size was used. An aluminum plate was cut out to cover its bottom and to fixate all of the housed components on. Rubber was used as an electrical insulator and spacer between the electrical compounds and the aluminum plate. The controlling board, a power supply and a DC/DC-converter were installed on the plate. The DC/DC-converter was necessary to convert the 27 V provided by the power supply to 12 V being the required voltage for the fans. On the sides of the box the following connections were implemented:

- three sockets for connecting Type K thermoelements
- four 2-pole sockets for the connections of the two transferline heatings, for the connection of the cooling tower heating and for the "ready"-readout from the gas chromatograph for measurement start
- a USB connection for connecting the Arduino on the board with a computer
- four 4-pole connections for possible use of the setup with PT100/1000 thermosensors

Additionally, a hole was cut out of the box to install a fan in order to prevent the electronics inside of the box from overheating. A picture of the construced box is shown in Figure 33, the cover was removed for presentation purposes.

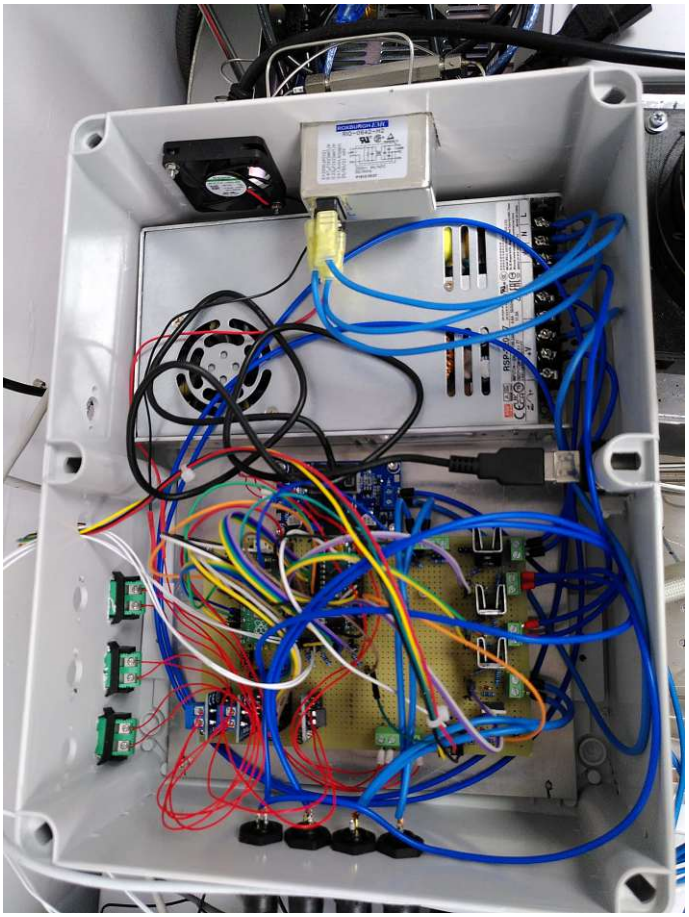

Figure 33: Top view of the "Plug-And-Play"-type box for controlling and connecting the cooling tower.

6.4 Terminology for Measurement Parameters

Since the measurement parameters differ from the ones of conventional gas chromatography those are explained in short in Table 6.

Table 6: Explanation of measurement parameters of the cooling tower.

Parameter	Explanation
Transferline temperature / °C	Temperature of the transferlines at the inlet and outlet of the cooling tower
Final run Temperature / °C	Temperature that outlet/cooling tower will reach at the end (highest temperature of the measurement)
Cooltime / s	Time span in which the fan of the cooling tower is cooling to achieve the negative thermal gradient

6.5 System Tests and Optimization

To evaluate the system's chromatographic performance, again a n-C_8- n-C_{20} standard in n-hexane with a concentration of 40 mg/l by *Supelco*^{TM}(Merck, Darmstadt, Germany, 04070- 5ml) was measured. Chromatograms were recorded with the *XCalibur* software by *ThermoFisher*^{TM}. For data presentation the .RAW files were ex-

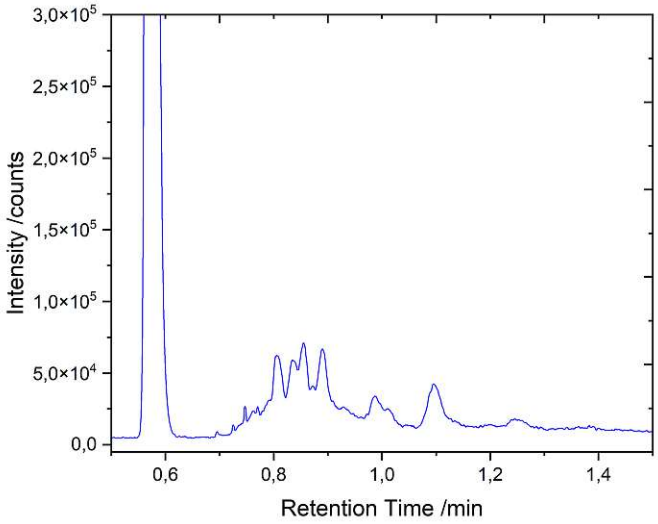

Figure 34: Cooling tower measurements with transferlines at 150 °C, MS interface temperature at 170 °C and a cooltime of 12 seconds.

ported and analyzed using Origin[2023].

For all measurements 1 µl of the standard was manually injected with a split ratio of 1:150. At first some measurements were performed to ensure that the setup is working properly. One of the first chromatograms is shown in Figure 34 showing that there definitely is some room for improvement. The peaks are badly resolved and the measurements take longer than in the initial setup (section 4).
As a result more measurements were performed at different temperatures. One of the exemplary chromatograms is depicted in Figure 35. The peaks are better resolved and the eluting bands are way smaller. The initial setup was able to separate n-octane to n-eicosane in twelve seconds. In this time span, only n-octane to n-tetradecane are separated and resolved with the DSQII Setup.
As a next step the final run temperature and the temperature of the transferlines of the cooling tower were increased to improve the speed of the measurement. To ensure resolution also the measurement parameters were optimized. All of the measurements were performed in single ion monitoring mode (SIM) to achieve the highest possible data acquisition rate. The resulting chromatogram is depicted in Figure 36.

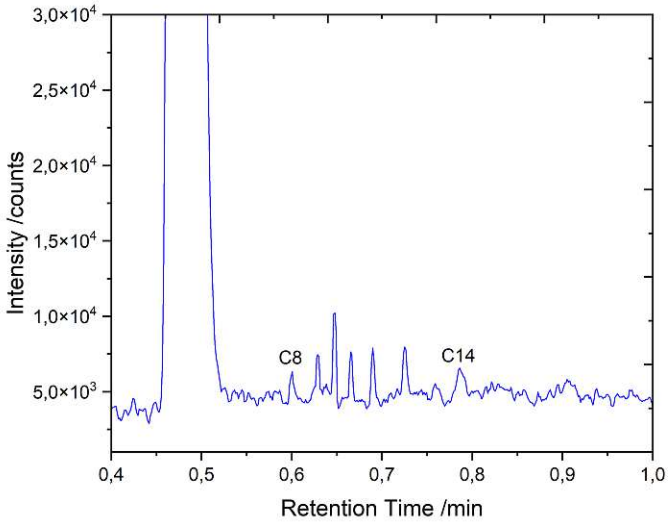

Figure 35: Cooling tower measurements with transferlines at 140 °C, MS interface temperature at 200 °C and a cooltime of 12 seconds.

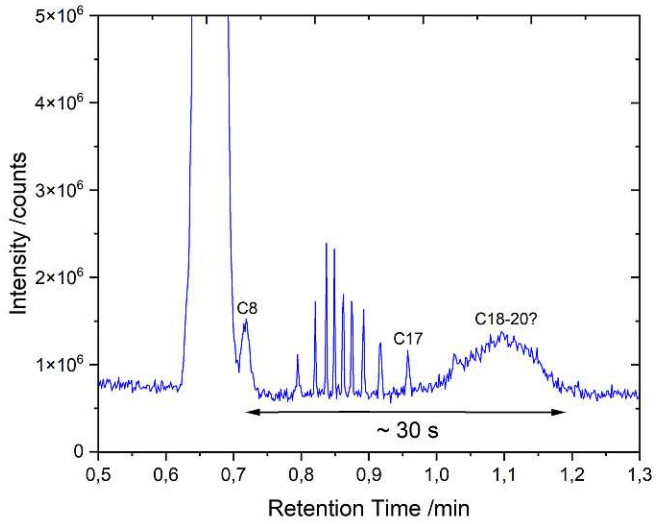

Figure 36: Cooling tower measurements with transferlines at 180 °C, MS interface temperature at 180 °C, outlet-run temperature at 140 °C and a cooltime of 3 seconds.

The peaks of n-octane to n-heptadecane were resolved properly only the peaks of the least volatile compounds (n-octadecane to n-eicosane) coeluted. So for the final measurements shown in this work the outlet run temperature was chosen higher than in Figure 36. The retention time of n-eicosane could not be determined because of the broadness of the coeluting peak, making the ∼30 seconds shown in Figure 36

only a rough estimation.

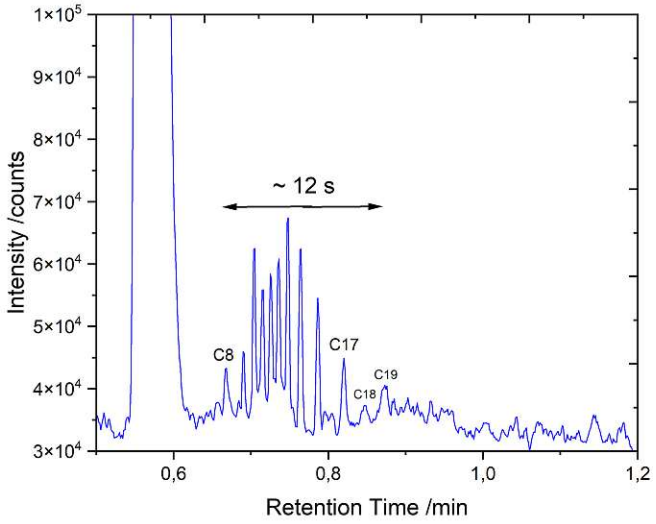

Figure 37: Cooling tower measurements with transferlines at 160 °C, MS interface temperature at 200 °C, outlet-run temperature at 160 °C and a cooltime of 3 seconds.

Figure 37 shows that the peaks from n-octane to n-nonadecane are resolved in the same timespan as the initial setup was able to resolve n-octane to n-eicosane. Again the retention time of n-eicosane could not be determined for the chromatogram shown in Figure 37. Unfortunately, the peaks show no baseline resolution as compared to Figure 16. This likely is a consequence of the limited data acquisition rate of the quadrupole mass spectrometer which also limits the resolution of the finally obtained chromatographic signal. Additionally, n-eicosane was still not eluting suggesting the presence of a coldspot in the measurement setup that should be resolved. This happened later in the other setups (sections 7 and 8). After this final measurement the work on the DSQII quadrupole was stopped with the exact reasons being listed in the following section.

6.6 Reasons for not Continuing with the DSQII

As can be seen from Figures 34 to 37, the scan speed of the quadrupole mass spectrometer was simply to low to fully resolve the peaks eluting from the cooling tower. It is only able to measure with a scan rate of 10000 amu per second. To circumvent this aspect, measurements in single ion monitoring mode (SIM) were performed to concentrate the scan rate on only selected masses. Unfortunately, even utilizing SIM mode did not provide satisfactory resolution of the homologous

series of the n-alkanes. The low acquisition rate results from the quadrupole's nature of scanning masses sequentially so its dwell time and speed do not allow to acquire a sufficient amount of data points for a peak. This is the first reason why the DSQII was not regarded as suitable for the following setups.

Additionally, from the beginning the ion source heating of the DSQII was defective. To prevent overheating and to control the heating rate, an external resistor was included in the heating circuit at already an earlier stage. This resistor had to be removed since its only effect was to drastically reduce the heating rate. As a result all of the measurements were performed at the highest temperature the ion source could reach at the time, fluctuating between 257 °C and 265 °C. The non-controllable ion source heating together with the slow scan speed of the quadrupole finally lead to abandoning the DSQII for subsequent work with the cooling tower.

7 Setup 3: Shimadzu 2010 GC with BID

Since the acquisition rate of the the detector shown in the second setup (section 6) was not sufficient for use in combination with the cooling tower, a different detector that provided a higher data acquisition rate was assessed and used. For this purpose the cooling tower was connected to a Tracera-GC-2010 Plus with a BID detector by Shimadzu (Duisburg, Germany).

7.1 Barrier Ionization Discharge Detector (BID)

The BID utilizes a helium plasma (excited helium atoms release photons with an energy of 17.7 eV when transitioning to the ground state) that is generated by applying high voltage to a dielectric chamber. The compounds eluting from the column are photo-ionized and then collected at the electrodes leading to peaks. Due to the high energy of the helium plasma almost every compound (apart from helium and neon) can be photo-ionized and therefore detected. The schematic cross section of the Bid used for Setup 3 and 4 in this work is shown in Figure 38. Not only is the BID capable of detecting fully oxidized carbon compounds (in contrast to the FID) but also is its acquisition speed higher than that of a quadrupole mass spectrometer. Its main disadvantage compared to the mass spectrometer is that peak assignment can only be done on the basis of the retention time since the detector does not provide any further information in addition to the intensity as a function of the retention time. [52, 53]

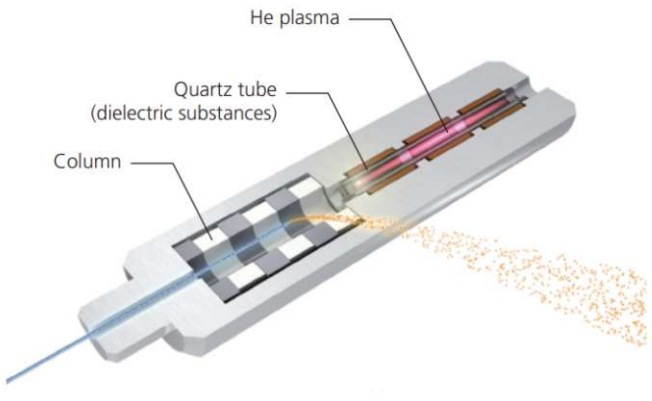

Figure 38: Schematic cross section of the BID detector used in this work [53].

7.2 Interfacing the Cooling Tower with the GC-BID

Connecting the cooling tower to the GC-BID was performed similarly to Setup 1 (chapter 4, Figure 15). The only difference is that the TGGC was connected to the injection and the detection unit of the GC-BID by leading the heated transferlines of the cooling tower through holes in the upper wall of the GC-BID. For heating the leading and trailing parts of the capillary column, the column was inserte into the oven of the GC-BID. The same electronics box was used as presented in setup 2. A sketch of the setup is illustrated in Figure 38, while a photograph taken of the setup is shown in Figure 40.

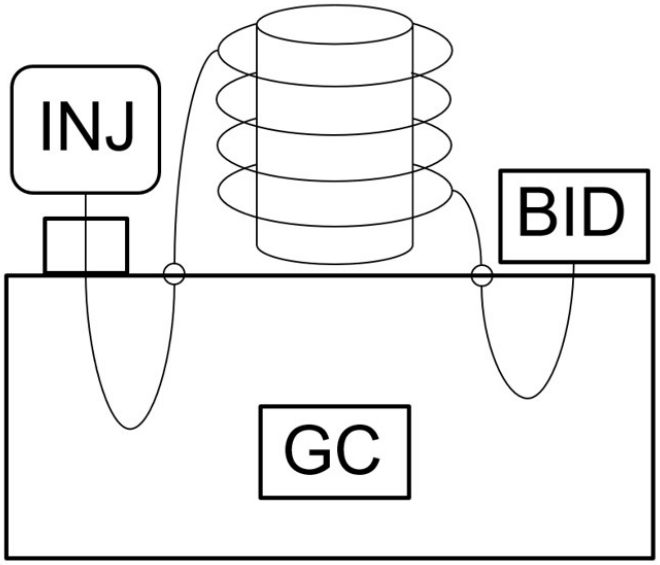

Figure 39: Schematic depection of the cooling tower connected to the GC-BID.

Figure 40: Photograph of the TGGC-BID.

7.3 System Tests and Optimization

For the test measurements the same capillary column and standard as shown in section 6 was used. The measurement conditions for each chromatogram will be summarized in the description of the figures.

7.3.1 Initial Measurements

One of the first measurements is depicted in Figure 41. Most of the peaks are overlapping using the settings shown in the figure description. Additionally, the baseline is unstable and the chromatogram shows overall low intensities. The main focus for the following measurements was to increase the retention of the early eluting peaks and to improve their resolution.

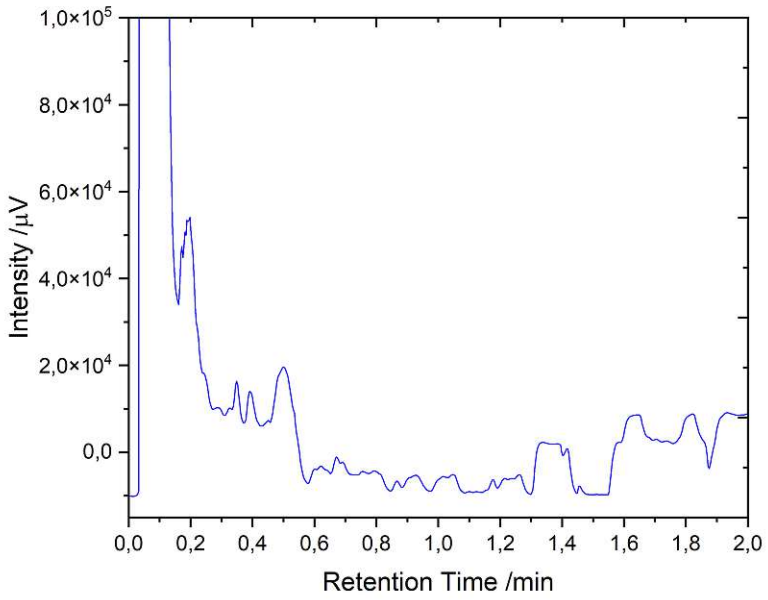

Figure 41: Chromatogram of one of the first measurements. Transferlines at 140 °C, column oven temperature at 200 °C, split 1:150, helium flow 1 ml/min and final run temperature at 150 °C.

7.3.2 Optimization Approaches

After varying the measurement parameters, the chromatogram shown in Figure 42 was one of the first chromatograms to show most of the peaks. The analyzed mixture was spiked with a solution containing n-decane, n-dodecane and n-hexadecane (hence the variation in peak intensities in the chromatogram). To resolve the peaks of the more volatile and therefore earlier eluting compounds the temperature ramp at the beginning was slowed down. As a result the measurement time drastically increased compared to the measurements presented in sections 4 and 6. The reduction of measurement time was the focus of the following optimization approaches.

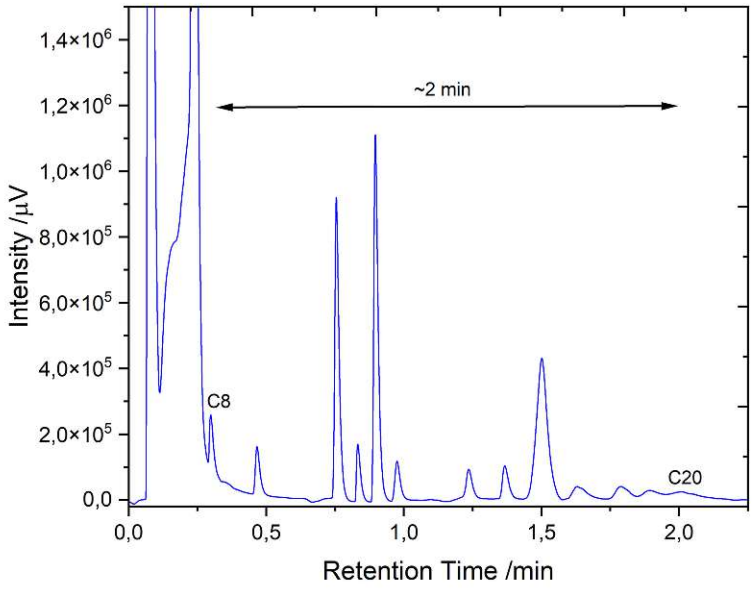

Figure 42: Chromatogram acquired with TGGC-BID. Transferlines at 180 °C, column oven temperature at 250 °C, split 1:250, helium flow 0.5 ml/min and final run temperature at 150 °C.

The measurement time in Figure 43 could already be reduced but the peaks show considerable tailing even at the beginning leading to the conclusion that the heating ramp at the beginning of the measurement is still too slow. Additionally, the distance between the peaks is large meaning that there is still room for acceleration of the measurement.

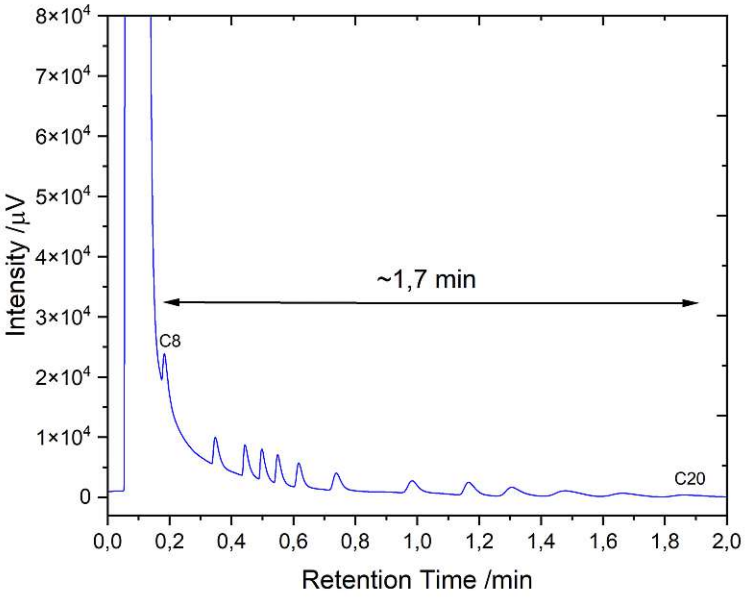

Figure 43: Chromatogram acquired with TGGC-BID. Transferlines at 180 °C, column oven temperature at 200 °C, split 1:200, helium flow 0.5 ml/min and final run temperature at 180 °C.

The heating rate was further increased to provide the result presented in Figure 44. It can be seen that baseline separation is no longer given and the peaks start overlapping again, although almost ideal cooling tower settings were used. After conferring with a service technician of Shimadzu's it was realized that the BID was not used at proper settings for analyzing peak widths as small as the ones eluting from the cooling tower. The acquisition rate of the BID was then tuned to 4 ms by the service technician after which a new optimization approach began for this setup. The optimization shown in this chapter was therefore performed correctly but the lacking data acquisition rate cannot be circumvented by enhancing chromatographic resolution since they are independent from each other.

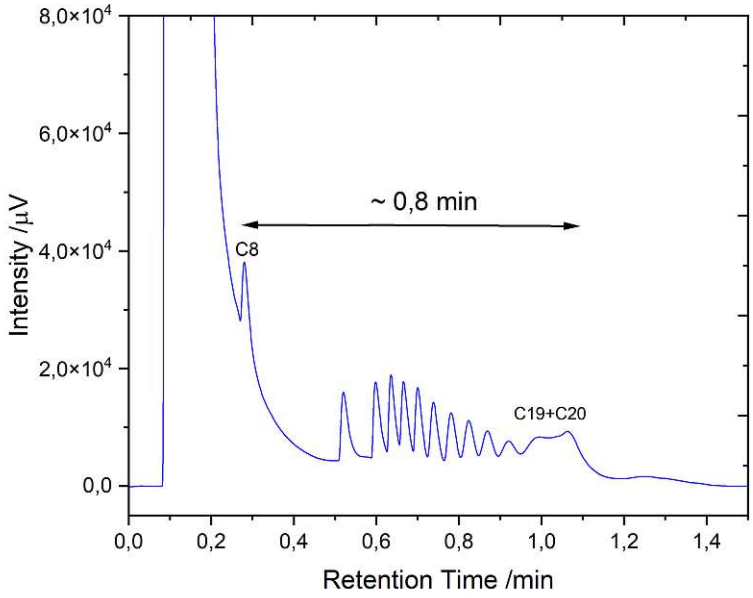

Figure 44: Chromatogram acquired with TGGC-BID. Transferlines at 180 °C, column oven temperature at 200 °C, split 1:200, helium flow 0.5 ml/min and final run temperature at 180 °C.

7.3.3 Measurements with Faster Scanning Rate

Utilizing the faster scanning rate it was tried to further reduce measurement time. The first result is shown for a sample spiked with n-decane, n-dodecane, n-tetradecane and n-hexadecane. The elution speed, peak width and measurement time was drastically enhanced compared to Figure 44. Unfortunately, the peaks of n-nonadecane and n-eicosane are still coeluting and were not separated. It is possible that by installing the cooling tower to the new instrument a coldspot was created that before was not recognizable.

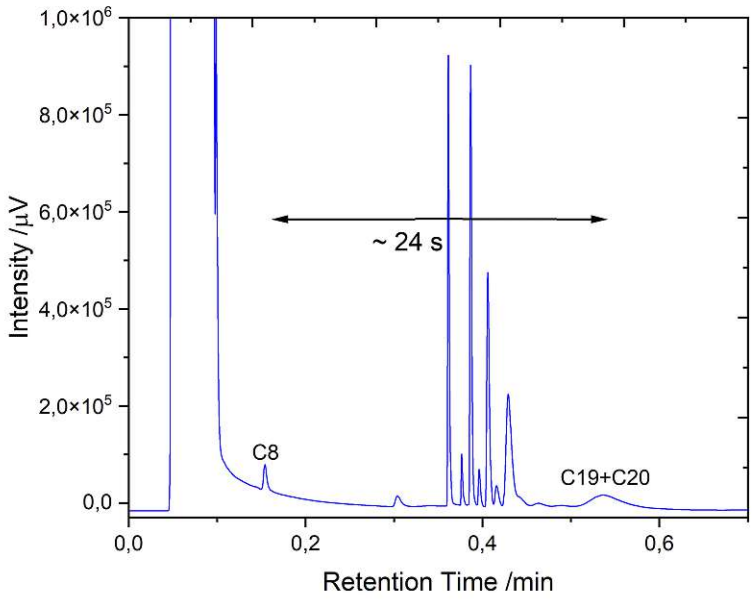

Figure 45: Chromatogram of the n-alkane standard spiked with n-decane, n-dodecane, n-tetradecane and n-hexadecane acquired with TGGC-BID. Transferlines at 180 °C, column oven temperature at 200 °C, split 1:200, helium flow 0.5 ml/min and final run temperature at 180 °C.

For the last measurement presented the temperature of the transferlines and the final run temperature were increased again. This resulted in faster elution times and sharp peaks and was leading to the first results similar to the ones presented in chapter 4. The increased noise results from the characteristics of the detectors (FID vs. BID). Still n-eicosane is not visible or the peak is at least that broad that it is not distinguishable from the noise. More measurements would be necessary for finally reaching optimal conditions for the TGGC-BID and also the cold spot needs to be identified and eliminated in the new instrumental setup.

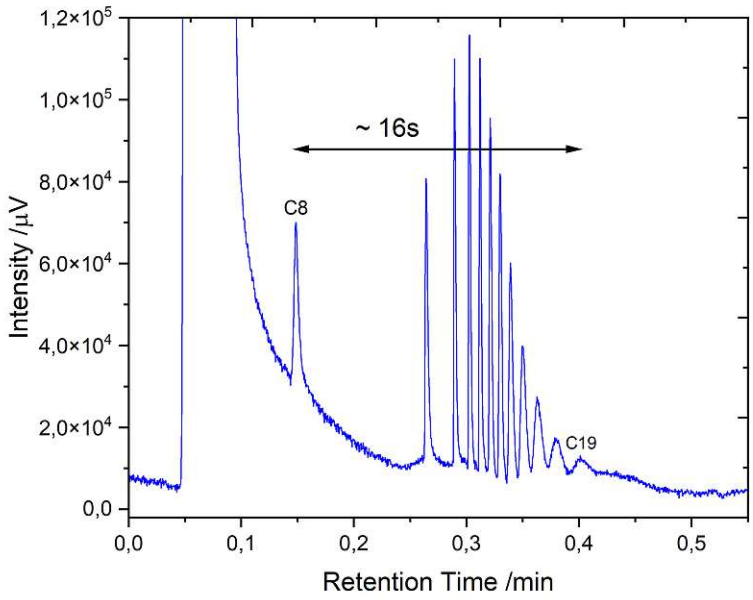

Figure 46: Chromatogram acquired with TGGC-BID. Transferlines at 210 °C, column oven temperature at 250 °C, split 1:150, helium flow 0.5 ml/min and outlet run temperature at 200 °C.

7.4 Conclusion and Next Steps

As can be seen from the last measurements (Figure 45 and 46) resolution and speed could be improved after adapting the detector for enabling higher scanning rates. Since n-eicosane is still eluting as a very broad peak (if it elutes at all) a coldspot at the in- or outlet is suspected (later resolved in section 8). At this point in time more optimization measurements for the setup were planned but laboratory space was made available by our research partner AIT to proceed with the adaptation of the system for the electrolyte measurements (shown in section 8).

8 Setup 4: Shimadzu 2010 GC with BID with PLOT column

As described in Sections 1.1 and 1.2 the main aim of our research group within the scope of the project was to develop a real time monitoring method for in-situ use with lithium-ion batteries. At AIT a special chamber in which LIBs can be charged and discharged at much higher than typical rates is at hand. With this setup, pouch cells can be directly connected to a transferline leading to the GC-MS enabling on-line measurements of their volatile emissions. Until now, acquiring chromatograms with this setup takes between 25-35 minutes while one charging cycle is performed every 20 minutes (charging at 3C). To obtain time resolved information analysis of the volatile species a fast measurement technique has to be employed. This can either be performed by performing multiplexing or on-line spectroscopy. In this work the fast TGGC-BID system shown in chapter 7 will be implemented and adapted for this purpose.

8.1 Experimental Setup

In order to analyze the gas phase extracted from pouch cells or from the headspace of gastight vials almost the same setup as presented in chapter 7 was used. The main difference was the change in the separation column which was necessary to ensure sufficient retention of the gaseous species. Instead of the Supelco SLB5-ms capillary column a porous layer open tubular (PLOT) column (Rt-Q-BOND PLOT Column by Restek Corporation) whose specifications are illustrated in Table 7 was installed.

Table 7: Column specifications of Rt-Q-Bond PLOT Column.

Column Specifications	
Name	Rt-Q-BOND PLOT
Length / m	5
d_f / µm	10
Inner diameter / mm	0.32
Temperature range / °C	-60 to 300
Stationary phase	Divinylbenzene

8.2 Test Measurements for PLOT Column with Liquified Petroleum Gas (LPG)

In order to determine the functionality and stability of the system as it is, test measurements with liqiuified petroleum gas (LPG) were performed. Up to this point the demonstration of the system's functionality has been conducted by measuring the "gold standard" for GC, a C_8 to C_{20} standard. Since this standard is not suitable for a PLOT column a different sample had to be used. The sample of LPG, a mixture of C_1 to C_5 n- and i-alkanes, whose volatility is ideal for testing PLOT columns. Two of the first test measurements are depicted in Figures 47 and 48. The measurement conditions are summarized in Table 8. The peak assignment was performed by comparing the chromatograms to Wan [54] who performed fast GC measurements of LPG on a PLOT column.

Table 8: Measurement parameters for the first LPG measurements.

Condition	Measurement A	Measurement B
Injection volume / µl	5	5
Transferline temperature / °C	140	150
Cooltime / s	3	3
Final run temperature / °C	140	150

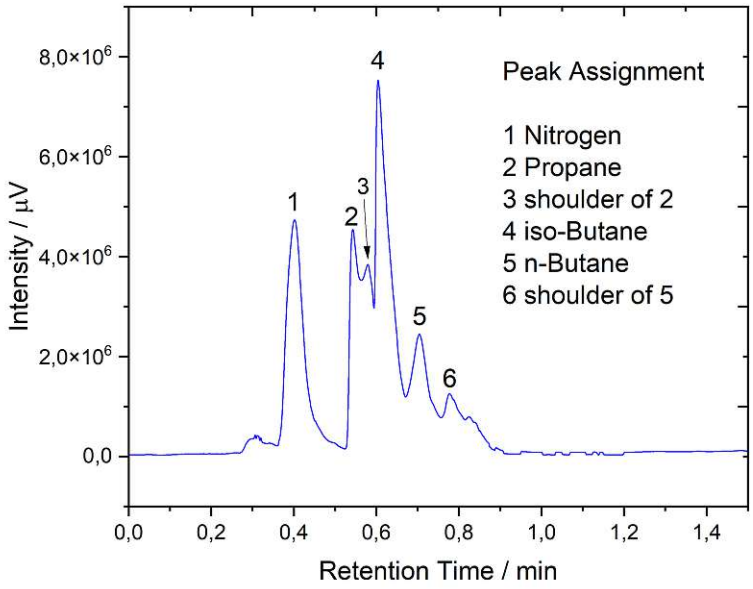

Figure 47: Chromatogram of the first LPG measurement (A). Peak assignment was performed by comparing with [54].

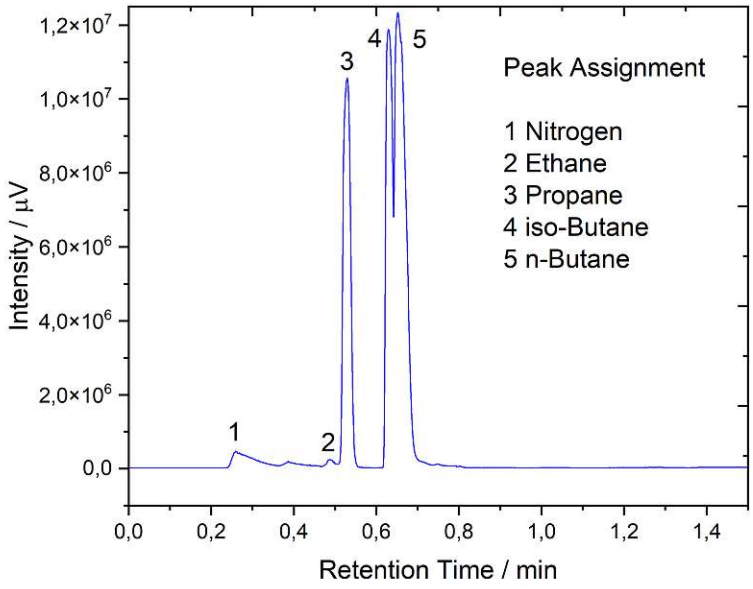

Figure 48: Chromatogram of one of the LPG measurement (B). Peak assignment was performed by comparing with [54].

8.2.1 Optimization and Reduction of Cold Spots

As evident from Figures 47 and 48 the resolution and as a result the peak width need to be enhanced. The peak broadening was thought to be caused by cold spots along the Cooling Tower which had to be eliminated. Unfortunately, discovering possible coldspots is no trivial task.

Two major cold spots have (accidentally) been detected by replacing our default Type-K thermoelements (Setup 1) with micro-thermoelements. These should decrease the risk for cold spots at the point of temperature measurement as their thermal mass is significantly lower. Additionally, the thermoelements were installed using a thermally conductive adhesive replacing the previous fixation by Kapton tape and thermal paste. Since the measuring probe is considerably smaller (0.076 mm in diameter) we were able to place the probe in the nearest vicinity of the heating supply of the TPGC and of the transferlines. Performing measurements with the new thermoelements showed that a severe cold spot (temperature difference of up to 40 °C) is located between the endpoint of the transferline heating and the beginning of the TPGC heating.

In order to resolve these issues the alligator clips of the TPGC heating were replaced, since one major problem was the inability to place the alligator clip directly next to the area heated by the transferline heating. To overcome this problem the cable of the TPGC heating was crimped to the steel capillary directly behind the heating of the transferline. The overlap of those two heating areas ensured the removal of the coldsport. This approach was adopted for both, the inlet and the outlet side.

Nevertheless, the new fixation bore a risk for short circuits. After installing the housing of the cooling tower which applied mechanical stress to the connection the heating circuit of the transferline (outlet side) and the heating circuit of the cooling tower contacted resulting in a tremendous overheat of the transferline. In order to overcome this problem, the electrical insulation of the connection was done more thorougly and the slits of the housing for the heating supply cables were enlarged to reduce risk of mechanical stress.

Afterwards more LPG measurements were performed with the newly enhanced setup. Measuring the temperatures on the locations of the previously identified cold spots led to a satisfying result. The same is true for the following measurements.

After a few more optimization steps the final chromatogram of the optimization procedure was acquired. The resulting chromatrogram is depicted in Figure 49 and its measurement parameters are reported in Table 9. The peak width, intensity and runtime were found to be sufficient to proceed with the electrolyte measurements.

Table 9: Measurement parameters for the final LPG measurement.

Condition	Measurement
Injection volume / µl	5
Transferline temperature / °C	150
Cooltime / s	3
Final run temperature / °C	150

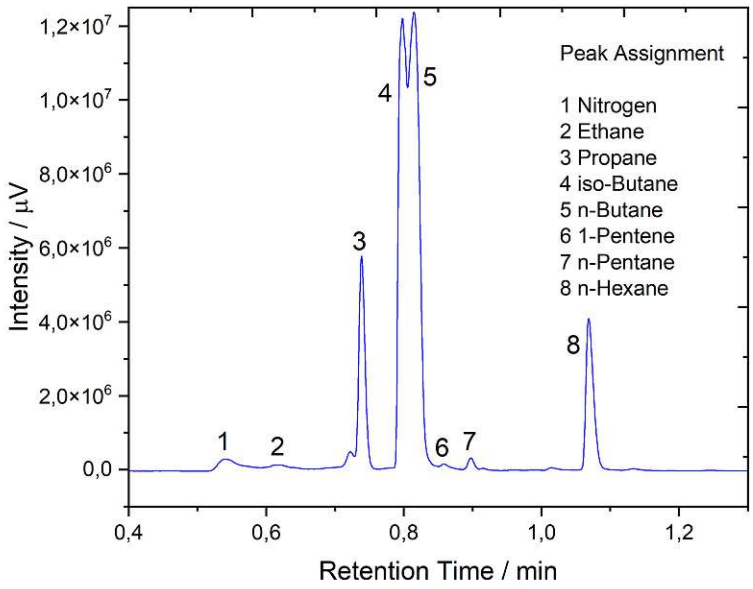

Figure 49: Chromatogram of one of the final LPG measurements using the parameters reported in Table 9. Peak assignment was performed by comparing with [54].

8.3 First Electrolyte Measurements

Since it was planned to perform operando measurements in the course of charging cycles of pouch cells in the battery abuse chamber, the setup had to be adapted to real life samples which was realised by measuring the headspace, the gaseous phase over the liquid phase of an electrolyte in a headspace vial. The electrolytes contained 1 mM lithium hexafluorophosphate ($LiPF_6$) dissolved in etylene carbonate (EC), diethyl carbonate (DEC), ethyl methyl carbonate (EMC) etc. depending

on the sample. By evaluating the resulting chromatograms, the system should be optimized towards electrolyte samples. Two of the chromatograms for these optimization approaches are shown in Figures 50 and 51. Both of these were acquired with transferline temperatures of 150 °C and final run temperatures of 120 °C. For peak assignment both chromatograms were compared to a reference measurement presented in the appendix (Figure 57).

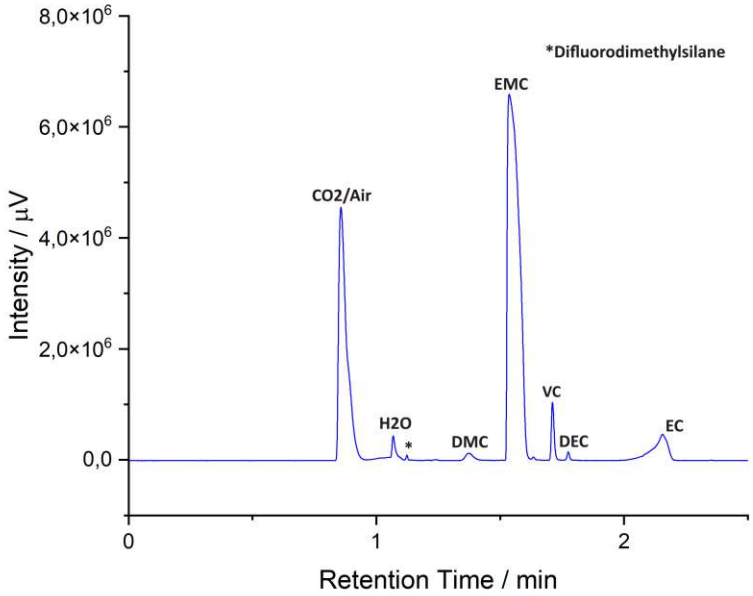

Figure 50: Chromatogram of an electrolyte sample (A).

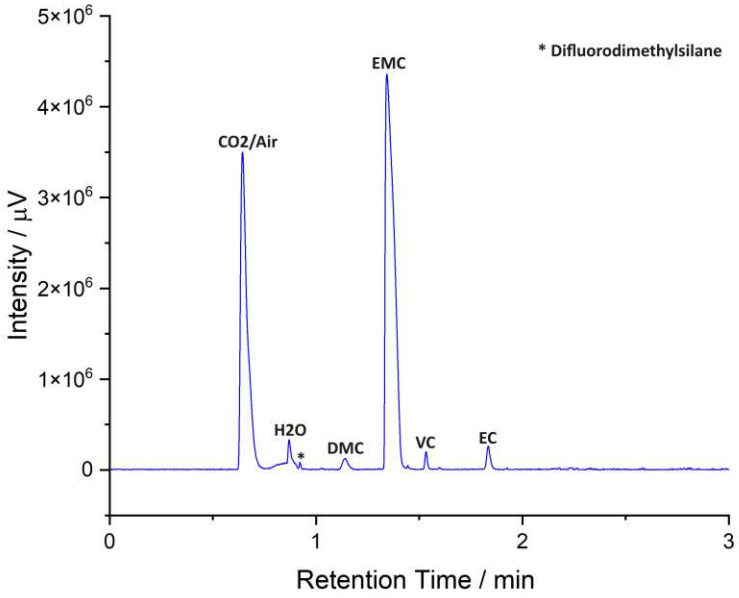

Figure 51: Chromatogram of an electrolyte sample (B).

Since the comparison with the reference yielded satisfactory results, an experiment with a different electrolyte was conducted, the same one which will later be used in the dynamic exerpiments (section 8.4). After optimizing the measurement conditions, an EC/DEC (1:1) sample with 1 mM $LiPF_6$, was measured and compared to a reference measurement provided by AIT in order to perform peak assignment (Figure 58 in the appendix). To increase the speed of the measurements the outlet run temperature was set at 200 °C and the injection volume was increased to 300 µl using a split ratio of 1:8. The transferlines were held at 200 °C. The resulting chromatogram of the EC/DEC sample is reported in Figure 52 together with the assumed peak assignments. The chromatogram matched sufficently with the reference in the appendix (Figure 58) which is why this electrolyte sample was used for the dynamic experiment. For assigning the remaining peaks and to validate the assumptions measurements with a different detector (one that allows analyte determination) e.g. a mass spectrometer should be performed. Nevertheless, the set measurement parameters were then used to perform the dynamic experiment shown in section 8.4.

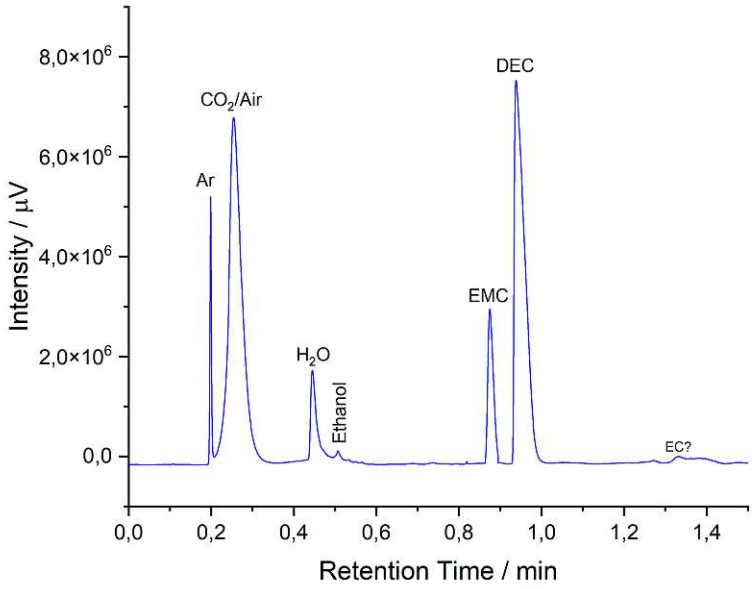

Figure 52: Chromatogram of EC/DEC sample. The measurement conditions are reported in Table 10.

8.4 Dynamic Experiment for Monitoring Electrolyte Decomposition

Originally it was planned to install the cooling tower module on the GC-MS at AIT since it is directly linked to the battery abuse chamber via a heated transferline. Unfortunately, the instrument was fully booked at the time of performing these experiments, thus prohibiting the installation of the cooling tower module on the GC-MS setup. This is why an alternative experiment had to be proposed in order to show the time resolution and suitability of the cooling tower for real-time monitoring operando measurements studyding the chemistry of lithium ion batteries.

In order to prove the possibility to do time resolved measurements a dynamic experiment with the EC/DEC electrolyte was conducted. 300 µl of this electrolyte were filled into a 10 ml headspace vial under inert conditions (in the glove box and under argon atmosphere). The idea was that the addition of water to the sample should initiate a kind of hydrolysis reaction. At first, a sample of the pure electrolyte was taken and a chromatogram was acquired (Figure 52, reaction time t = 0 min). Immediately after, 1 % water was added to the vial to initiate hydrolysis. From this point on samples were taken, injected and measured every ten minutes in a time span of 100 minutes (t = 100 min). The parameters of the measurement are shown

in Table 10.

Table 10: Measurement parameters for the dynamic experiments.

Dynamic measurements	
Vial volume / ml	10
Vial liquid phase / µl	300
Injection volume / µl	300
Split ratio	1:8
Transferline temperature / °C	200
Cooltime / s	3
Final run temperature / °C	200

The stacked chromatograms are depicted in Figures 53 to 55. The times "t" are the total reaction time i.e. the time that has passed since the addition of 1 % Water. The peaks for air and CO_2 have been cut out for the sake of clarity of the presentation. Additionally, the measurement for the reaction time of 60 minutes has been left out since an error occured with regard to data acquisition.

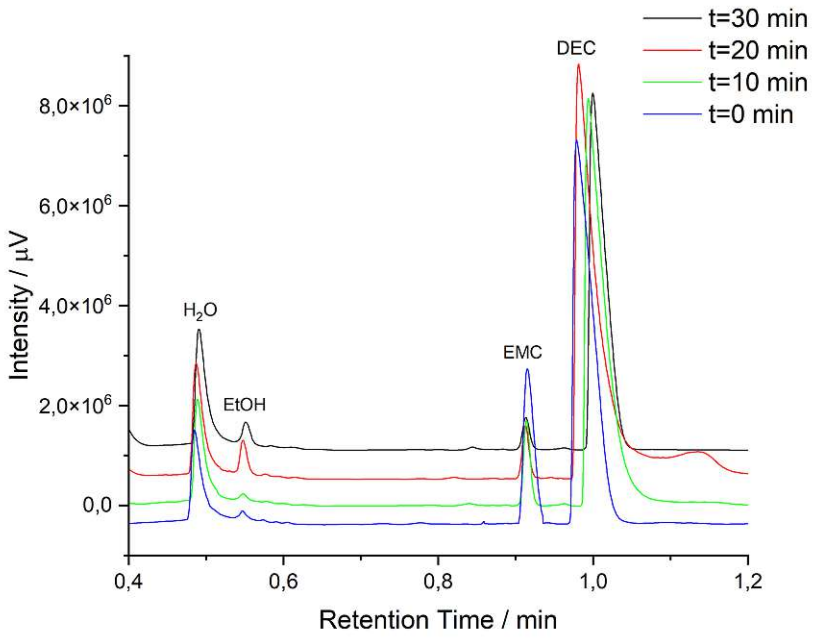

Figure 53: Chromatograms of the dynamic experiment for t = 0 to t = 30 min.

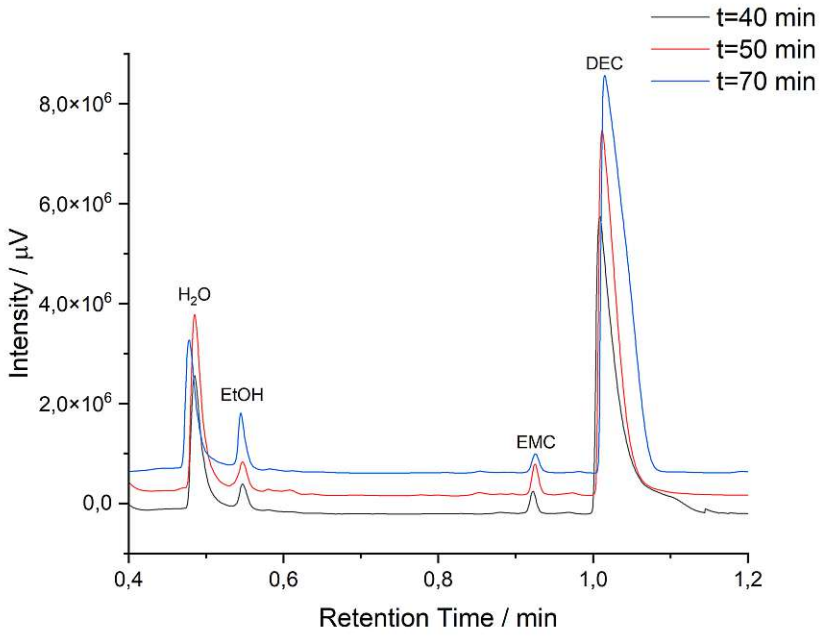

Figure 54: Chromatograms of the dynamic experiment for t = 40 to t = 70 min.

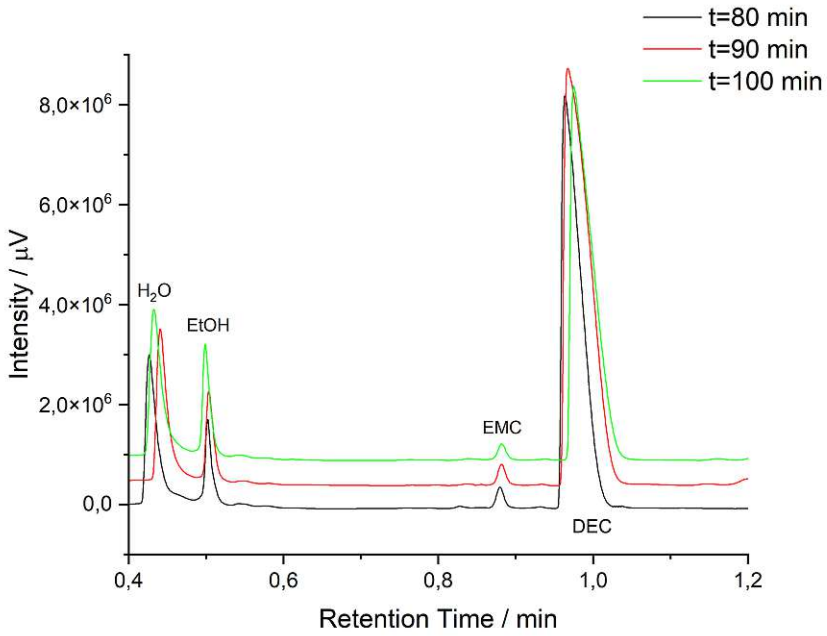

Figure 55: Chromatograms of the dynamic experiment for t = 80 to t = 100 min.

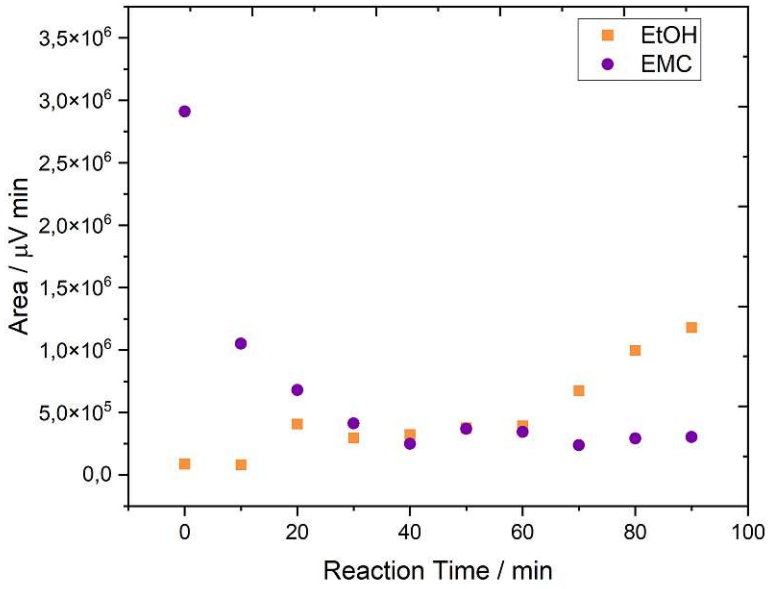

Figure 56: Plot of the peak areas of Ethanol (EtOH) and ethyl methyl carbonate (EMC) against the reaction time.

8.5 Discussion

From the Figures 53 to 55 it is evident that over the course of the reaction the ethanol content is constantly increasing. The oppsosite is true for EMC which is drastically decreasing until a reaction time of 30 minutes. From there on it almost remains constant. This is underlined by the plot of their respective peak areas against the reaction time (Figure 56). The trend shown in Figure 56 suggests that an acidic ether cleavage might take place induced by the increasing concentration of hydrogen fluoride due to the degradation of $LiPF_6$ initiated by the addition of water.

In order to validate the results and to assign smaller peaks which were not assigned, the use of the GC-MS would be crucial to acquire structural information in addition to the qualitative information provided by the retention time. The ideal solution would be to determine the retention times and structures of all eluting compounds using the cooling tower TGGC module with the GC-MS and then perform quantification using the installed TGGC-BID for quantification.

Although measurements were performed only once every ten minutes, data acquisition would have been possible at a rate of one chromatogram every 3-4 minutes. This results from the fact that headspace measurements executed within our re-

search group showed that the headspace of a 10 ml vial takes approximately ten minutes to equilibrate after taking a sample. Furthermore, looking at the intensities of the chromatograms shown in this section, it is evident that the amound of sample introduced could be decreased. This would reduce the impact on cell chemistry in the course of operando measurements considering that 300 µl of gas phase would be removed from the cell every 3-4 minutes.

9 Summary

9.1 Implementation of a "Plug-and-Play" Concept

In this work a temperature gradient gas chromatograph based on the principle of Boeker et al.[15] and based on the work of Mueller [2] was modularized and developed into a "plug-and-play" concept enabling simple and fast installation to gas chromatographs from different producers. The feasibility of the modular concept was shown by the installations of the cooling tower in chapters 4 to 8.

9.2 Simulation of the TGGC

By performing isothermal measurements in a temperature range from 50-220 °C thermodynamical values for n-octane to n-eicosane were calculated. Based on these values a database for the simulation of the TGGC separation was created. A simulation of the cooling tower setup has then successfully been carried out with the GasChromatographySimulator provided by Leppert [50]. The theoretical results were compared to the experiment. As a result the peak broadening effects of n-octane and n-nonane were explainable. Additionally, the early elution of n-octane compaired to the other n-alkanes of the homologous series was understood.

9.3 Coupling to a Mass Spectrometric Detector

In order to prepare the cooling tower for the experimental setup at hand at AIT the TGGC module was successfully interfaced with a Thermo DSQII quadrupole mass spectrometer. An Agilent 6890-N was used as injection and flow regulation unit while the mass spectrometer was used as a detection unit. After providing the system with a suitable transferline heating measurements of a n-octane to n-eicosane standard have successfully been conducted. After optimizing the cooling tower measurement conditions it was, nevertheless, concluded that the scanning rate of the quadrupole mass spectrometer was too slow for the small peak widths of the TGGC setup and needed to be replaced by a detector with better time resolution. This was achieved with the BID. For comparison: with a scan range of for example 400 amu and a scan speed of 10000 amu/sec, a scan rate of 25 Hz (= 40 ms per spectrum) can be achieved. Additionally, a settling time of ∼10 ms per scan has to be taken into account resulting in a scan rate of ∼20 Hz. Considering that the peak widths for the TGGC lie between 20 - 250 ms, the acquisition rate was definitely too slow. The BID on the other hand could be tuned towards an acquisition rate of 4 ms making it the more suitable detector.

9.4 Adaptions for Use With Electrolyte Samples

After connecting the cooling tower to a detector with a sufficiently high data acquisition rate, the system was adapted for the analysis of electrolyte samples. At first, the system's performance was checked, after switching to a PLOT column, using LPG. Adjustments were made to the setup as well as coldspots removed. Next, by injecting and measuring electrolytes, the measurement conditions were optimized for real-time monitoring as aimed for in the OPERION project (section 1.1)

9.5 Time-resolved Electrolyte Measurements

Lastly, the coupling to lithium-ion batteries at AIT had to be realized in order to prove the system's claimed suitability for real-time monitoring and in-situ analysis. The connection of the cooling tower module to AIT's battery analysis setup was not possible in the time frame of this thesis. As an alternative, a dynamic experiment was carried following the degradation of an electrolyte sample after the addition of water. It was shown, that measurements can theoretically be performed every 3-4 minutes meaning a tenfold increase in time resolution, taking into consideration that the reference measurements at AIT's GC-MS setup take ∼40 minutes (including equilibration of the GC-MS). Installing the cooling tower would therefore enable to acquire approximately 5 chromatograms per charging cycle (20 minutes, since the charging rate is 3C).

10 Outlook

Having demonstrated the capability the capability of the TGGC-BID system for fast highly time-resolved measurements by monitoring the electrolyte decomposition, the system is now ready for online measurements at AIT. As soon as the GC-MS is available again the cooling tower module should be connected to it to evaluate its performance in in-situ measurements of volatile species created in electrochemical cycling experiments of LIBs. The cooling tower's short measurement time should provide the user with information with high time resolution and should help understanding degradation and aging mechanisms in the cells.

Apart from its application with LIBs, the cooling tower could be used for various other applications requiring fast gas chromatography. Due to its modular concept it can be easily installed to any conventional gas chromatograph and thereby implemented into any routine procedure for example for the online analysis of natural gases or fuel. In routine analysis it could highly increase sample throughput while increasing resolution and maintaining sensitivity.

For further optimizing the current experimental setup as it is the temperature measurements should be performed remotely using e.g. infrared sensors to decrease the risk of cold spots. Additionally, the design of the clamps made out of iron wire could be improved to decrease the contact area between steel capillary and each of the clamps to reduce heat exchange which again could result in cold spots. Furthermore, for ensuring faster cooling and to increase the reproducibility of the experiment, the cooling tower could be installed in a housing that can be flushed with thermostated air.

The idea of commercialising the cooling tower was never grasped, since its concept and setup are too closely linked to the setup shown and commercialised by Boeker. [29] In the meantime work in our research group focused on the development on another TGGC setup : The "Wavemaker". It utilizes a sawtooth gradient for optimal performance and separates components based on their equilibrium temperature. Its setup is currently undergoing the patenting process. At the moment, a part of the research group is working on possible applications of the "Wavemaker". One application could be to connect it to the GC-BID instead of the cooling tower to see its performance with electrolyte samples. Since its speed and chromatographic performance (Klampfl et al., to be published) in the measurements of a n-C_8 to n-C_{20} standard surpassed the cooling tower, it should be put to test in applications requiring good time resolution.

11 References

[1] www.ait.ac.at. *OPERION - AIT Austrian Institute Of Technology*. de. URL: https://www.ait.ac.at/themen/battery-materials-characterization/projekte/operion (visited on 11/04/2023).

[2] Robert Müller. „Design and Construction of a Thermal Gradient Module for Gas Chromatography“. In: Master Thesis, Technische Universität Wien, Vienna, Austria (June 2021).

[3] Kazunori Ozawa. „Lithium-ion rechargeable batteries with LiCoO2 and carbon electrodes: the LiCoO2/C system“. In: *Solid State Ionics* 69.3 (Aug. 1994), pp. 212–221. DOI: 10.1016/0167-2738(94)90411-1. (Visited on 11/04/2023).

[4] Reiner Korthauer, ed. *Lithium-Ion Batteries: Basics and Applications*. en. Berlin, Heidelberg: Springer Berlin Heidelberg, 2018. ISBN: 978-3-662-53069-6 978-3-662-53071-9. DOI: 10.1007/978-3-662-53071-9. (Visited on 11/04/2023).

[5] Gunther Bohn et al. „High-resolution Interferometric Measurement of Thickness Change on a Lithium-Ion Pouch Battery“. In: *IOP Conference Series: Earth and Environmental Science* 281 (June 2019), p. 012030. DOI: 10.1088/1755-1315/281/1/012030.

[6] Ulf Ritgen. *Analytische Chemie I*. de. Berlin, Heidelberg: Springer Berlin Heidelberg, 2019. ISBN: 978-3-662-60494-6. DOI: 10.1007/978-3-662-60495-3. (Visited on 11/04/2023).

[7] Hans-Joachim Hübschmann. *Handbook of GC-MS: Fundamentals and Applications*. en. Google-Books-ID: HoS4CAAAQBAJ. John Wiley & Sons, Apr. 2015. ISBN: 978-3-527-67432-9.

[8] Manfred H. Gey. *Instrumentelle Analytik und Bioanalytik: Biosubstanzen, Trennmethoden, Strukturanalytik, Applikationen*. de. Berlin, Heidelberg: Springer Berlin Heidelberg, 2021. ISBN: 978-3-662-63952-8. DOI: 10.1007/978-3-662-63952-8. (Visited on 02/05/2022).

[9] Richard Evers. „Development of a Liquid Chromatography Ion Trap Mass Spectrometer Method for Clinical Drugs of Abuse Testing with Automated On-Line Extraction Using Turbulent Flow Chromatography“. PhD thesis. Portsmouth, UK: University of Portsmouth, Sept. 2014. DOI: 10.13140/2.1.2125.1367.

[10] Robert L. Grob and Eugene F. Barry. *Modern Practice of Gas Chromatography*. en. Google-Books-ID: 2L_H2l5STa8C. John Wiley & Sons, Aug. 2004. ISBN: 978-0-471-65115-4.

[11] Harold M. McNair. *Basic Gas Chromatography, 3rd Edition | Wiley*. en-us. URL: https://www.wiley.com/en-us/Basic+Gas+Chromatography%2C+3rd+Edition-p-9781119450757 (visited on 11/05/2023).

[12] Erwin Rosenberg, Bernhard Klampfl, and Robert D. Müller. „Negative Thermal Gradient Gas Chromatography". In: (2023). Publisher: IntechOpen. URL: https://www.intechopen.com/online-first/86699 (visited on 11/04/2023).

[13] Wayne A. Rubey. „A different operational mode for addressing the general elution problem in rapid analysis gas chromatography". en. In: *Journal of High Resolution Chromatography* 14.8 (Aug. 1991), pp. 542–548. DOI: 10.1002/jhrc.1240140806. (Visited on 11/04/2023).

[14] Bernhard Klampfl. „Fast Gas Chromatography with Development of a Negative-Thermal Gradient GC for the Study of Volatile Products Formed in Lithium-Ion Batteries". In: 26. International Symposium on Separation Sciences (ISSS 2022), Ljubljana, July 2022.

[15] Peter Boeker and Jan Leppert. „Flow Field Thermal Gradient Gas Chromatography". en. In: *Analytical Chemistry* 87.17 (Sept. 2015), pp. 9033–9041. DOI: 10.1021/acs.analchem.5b02227. (Visited on 09/11/2023).

[16] Jesse Alberto Contreras. „Axial Temperature Gradients in Gas Chromatography". en. PhD thesis. Provo, Utah, USA: Brigham Young University, Dec. 2010.

[17] Jan Leppert et al. „Hyperfast Flow-Field Thermal Gradient GC/MS of Explosives with Reduced Elution Temperatures". en. In: *Analytical Chemistry* 90.14 (July 2018), pp. 8404–8411. DOI: 10.1021/acs.analchem.8b00900. (Visited on 11/05/2023).

[18] M. Fatscher. „Method using a [Chromatography] in which the column temperature is constant with time and varies exponentially along the longitudinal Abscissa". In: *Sciences Chimiques* 273 (1971), pp. 1042–1046.

[19] M. Fatscher and J. M. Vergnaud. „Use in quantitative analysis of gas chromatography methods with established longitudinal temperature gradient with or without temperature programming". In: *Analusis* 1 (1972), pp. 231–233.

[20] David C. Fenimore. „Gradient temperature programming of short capillary columns". In: *Journal of Chromatography A* 112 (Jan. 1975), pp. 219–227. DOI: 10.1016/S0021-9673(00)99955-2. (Visited on 11/04/2023).

[21] Wayne A. Rubey. „Operational theory and instrumental implementation of the thermal gradient programmed gas chromatography (TGPGC) mode of analysis“. en. In: *Journal of High Resolution Chromatography* 15.12 (Dec. 1992), pp. 795–799. DOI: 10.1002/jhrc.1240151205. (Visited on 11/04/2023).

[22] Vivek Jain and John B. Phillips. „High-Speed Gas Chromatography Using Simultaneous Temperature Gradients in Both Time and Distance along Narrow-Bore Capillary Columns“. In: *Journal of Chromatographic Science* 33.11 (Nov. 1995), pp. 601–605. DOI: 10.1093/chromsci/33.11.601. (Visited on 11/04/2023).

[23] Vivek Jain and John B. Phillips. „Fast Temperature Programming on Fused-Silica Open-Tubular Capillary Columns by Direct Resistive Heating“. In: *Journal of Chromatographic Science* 33.1 (Jan. 1995), pp. 55–59. DOI: 10.1093/chromsci/33.1.55. (Visited on 11/04/2023).

[24] John B. Phillips and Vivek Jain. „On-Column Temperature Programming in Gas Chromatography Using Temperature Gradients along the Capillary Column“. In: *Journal of Chromatographic Science* 33.10 (Oct. 1995), pp. 541–550. DOI: 10.1093/chromsci/33.10.541. (Visited on 11/04/2023).

[25] Jesse Alberto Contreras. „Design and application of thermal gradient programming techniques for use in multidimensional gas chromatography-mass spectrometry (MDGC-MS)“. In: Master Thesis,University of Dayton, Ohio, USA (2004). (Visited on 11/04/2023).

[26] Jesse A. Contreras et al. „Dynamic thermal gradient gas chromatography“. In: *Journal of Chromatography A* 1302 (Aug. 2013), pp. 143–151. DOI: 10.1016/j.chroma.2013.06.008. (Visited on 11/04/2023).

[27] Peter Boeker. „Flow-field-induced temperature gradient gas chromatography“. en. US10641748B2. May 2020. URL: https://patents.google.com/patent/US10641748B2/en (visited on 11/05/2023).

[28] Miriam D. Chopra et al. „Residual solvent analysis with hyper-fast gas chromatography-mass spectrometry and a liquid carbon dioxide cryofocusing in less than 90ăs“. In: *Journal of Chromatography A* 1648 (July 2021), p. 462179. DOI: 10.1016/j.chroma.2021.462179. (Visited on 11/05/2023).

[29] HyperChrom S.A. *Technology*. en. URL: https://www.hyperchrom.com/GC/technology/ (visited on 11/05/2023).

[30] Karl Johan Åström and Tore Hägglund. *PID Controllers: Theory, Design, and Tuning*. Research Triangle Park, North Carolina: ISA - The Instrumentation, Systems and Automation Society, 1995. ISBN: 978-1-55617-516-9.

[31] Oliver Gibietz. *Temperaturregler Typen: Wie funktioniert ein PID-Regler?* de-DE. Feb. 2019. URL: https://temperatur-profis.de/temperaturregler/reglertypen-pid/ (visited on 11/03/2023).

[32] *PID Control and Derivative on Measurement Control Guru*. URL: https://controlguru.com/pid-control-and-derivative-on-measurement/ (visited on 11/03/2023).

[33] Jacob Fraden. „Temperature Sensors“. en. In: *Handbook of Modern Sensors: Physics, Designs, and Applications*. Ed. by Jacob Fraden. Cham: Springer International Publishing, 2016, pp. 585–643. ISBN: 978-3-319-19303-8. DOI: 10.1007/978-3-319-19303-8_17. (Visited on 11/03/2023).

[34] Joseph J. Carr. *Sensors and Circuits: Sensors, Transducers, and Supporting Circuits for Electronic Instrumentation, Measurement, and Control*. en. Google-Books-ID: z0NTAAAAMAAJ. PTR Prentice Hall, 1993. ISBN: 978-0-13-805631-5.

[35] *Thermoelement Typ K - Technische Informationen - TC GmbH*. URL: https://www.tcgmbh.de/thermoelemente/typ-k-thermoelemente.html (visited on 11/03/2023).

[36] *RS PRO PTFE Thermoelement Typ K, Ø 1/0.076mm x 500mm -75řC +260řC | RS*. URL: https://at.rs-online.com/web/p/thermoelemente/2209491 (visited on 11/03/2023).

[37] *Arduino - Home*. URL: https://www.arduino.cc/ (visited on 11/05/2023).

[38] M. S. Klee and L. M. Blumberg. „Theoretical and Practical Aspects of Fast Gas Chromatography and Method Translation“. en. In: *Journal of Chromatographic Science* 40.5 (May 2002), pp. 234–247. DOI: 10.1093/chromsci/40.5.234. (Visited on 11/05/2023).

[39] Bryan Karolat and James Harynuk. „Prediction of gas chromatographic retention time via an additive thermodynamic model“. en. In: *Journal of Chromatography A* 1217.29 (July 2010), pp. 4862–4867. DOI: 10.1016/j.chroma.2010.05.037. (Visited on 09/11/2023).

[40] Malcolm L. Peterson and Jules Hirsch. „A calculation for locating the carrier gas front of a gas-liquid chromatogram“. en. In: *Journal of Lipid Research* 1.1 (Oct. 1959), pp. 132–134. DOI: 10.1016/S0022-2275(20)39104-5. (Visited on 10/31/2023).

[41] T. Watanachaiyong, N. Jeyashoke, and K. Krisnangkura. „A Convenient Method for Routine Estimation of Dead Time in Gas Chromatography“. en. In: *Journal of Chromatographic Science* 38.2 (Feb. 2000), pp. 67–71. DOI: 10.1093/chromsci/38.2.67. (Visited on 10/31/2023).

[42] Jesús Eduardo Quintanilla-López, Rosa Lebrón-Aguilar, and JoséAntonio García-Domínguez. „The hold-up time in gas chromatography II. Validation of the estimation based on the concept of a zero carbon atoms alkane“. en. In: *Journal of Chromatography A* 767.1-2 (Apr. 1997), pp. 127–136. DOI: 10.1016/S0021-9673(96)01033-3. (Visited on 10/31/2023).

[43] Liejun Wu et al. „Determination and evaluation of gas holdup time with the quadratic equation model and comparison with nonlinear models for isothermal gas chromatography“. en. In: *Journal of Chromatography A* 1297 (July 2013), pp. 196–203. DOI: 10.1016/j.chroma.2013.04.078. (Visited on 10/31/2023).

[44] Fredrik Aldaeus, Yasar Thewalim, and Anders Colmsjö. „Prediction of retention times of polycyclic aromatic hydrocarbons and n-alkanes in temperature-programmed gas chromatography“. en. In: *Analytical and Bioanalytical Chemistry* 389.3 (Sept. 2007), pp. 941–950. DOI: 10.1007/s00216-007-1528-0. (Visited on 09/11/2023).

[45] Reynaldo César Castells, Eleuterio Luis Arancibia, and Angel Miguel Nardillo. „Regression against temperature of gas chromatographic retention data“. In: *Journal of Chromatography A* 504 (Jan. 1990), pp. 45–53. DOI: 10.1016/S0021-9673(01)89512-1. (Visited on 09/11/2023).

[46] E. C. W. Clarke and D. N. Glew. „Evaluation of thermodynamic functions from equilibrium constants“. en. In: *Transactions of the Faraday Society* 62.0 (Jan. 1966). Publisher: The Royal Society of Chemistry, pp. 539–547. DOI: 10.1039/TF9666200539. (Visited on 09/11/2023).

[47] Zoltan A. Fekete et al. „Temperature dependence of solvation heat capacities by gas chromatography“. en. In: *Analytica Chimica Acta* 549.1-2 (Sept. 2005), pp. 134–139. DOI: 10.1016/j.aca.2005.06.027. (Visited on 09/11/2023).

[48] Francisco Rex González. „Considerations on the temperature dependence of the gasliquid chromatographic retention“. en. In: *Journal of Chromatography A* 942.1-2 (Jan. 2002), pp. 211–221. DOI: 10.1016/S0021-9673(01)01351-6. (Visited on 10/31/2023).

[49] Leonid M. Blumberg. „Distribution-centric 3-parameter thermodynamic models of partition gas chromatography“. en. In: *Journal of Chromatography A* 1491 (Mar. 2017), pp. 159–170. DOI: 10.1016/j.chroma.2017.02.047. (Visited on 09/13/2023).

[50] Jan Leppert. „GasChromatographySimulator.jl“. en. In: *Journal of Open Source Software* 7.76 (Aug. 2022), p. 4565. DOI: 10.21105/joss.04565. URL: https://joss.theoj.org/papers/10.21105/joss.04565 (visited on 09/11/2023).

[51] Jürgen H. Gross. *Massenspektrometrie: Spektroskopiekurs kompakt*. de. Berlin, Heidelberg: Springer Berlin Heidelberg, 2019. ISBN: 978-3-662-58634-1 978-3-662-58635-8. DOI: 10.1007/978-3-662-58635-8. (Visited on 11/16/2023).

[52] Nicole Lock, Richard Whitney, and Clifford M Taylor. „New Applications Using GC BID Detector“. en. In: PITTCON2014 (2014). URL: https://gcms.labrulez.com/paper/3364.

[53] *Tracera - GC system with barrier discharge ionization detector (BID) (Shimadzu Europe) | EVISA's Instruments Database*. URL: https://speciation.net/Database/Instruments/Shimadzu-Europe/Tracera-GC-system-with-barrier-discharge-ionization-detector-BID-;i3134 (visited on 11/14/2023).

[54] Li Wan and Agilent Technologies. *Determination of Hydrocarbon Composition in Liquefied Petroleum Gas Using the Agilent GC Gasifier and the Agilent 990 Micro GC*. en. Oct. 2020.

12 List of Figures

13 List of Tables

14 Appendix

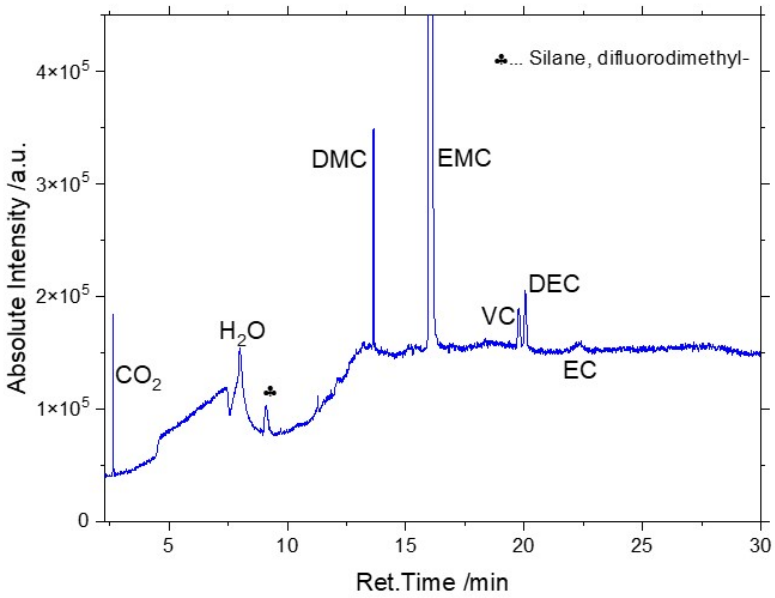

Figure 57: Reference chromatogram acquired for peak assignment of the EC/EMC electrolyte. Chromatogram was acquired with a GC-MS using headspace injection. (30 m PLOT column, 30 - 190 °C at 15 °C/min, 250 µl injection volume, headspace vial at 60 °C)

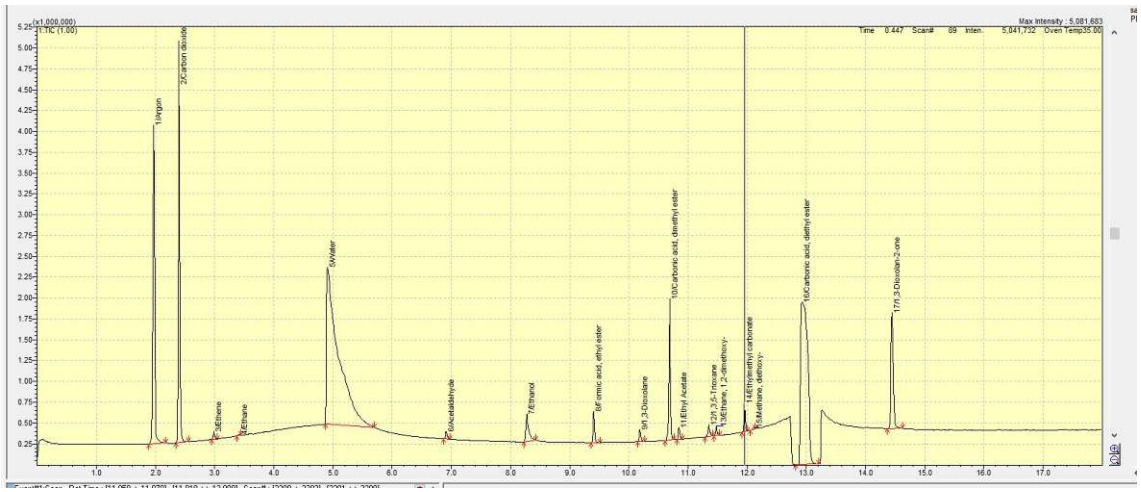

Figure 58: Reference chromatogram provided by AIT for peak assignment of the EC/DEC electrolyte. Chromatogram was acquired with a GC-MS. 30 m PLOT column, 30 - 190 °C at 15 °C/min.

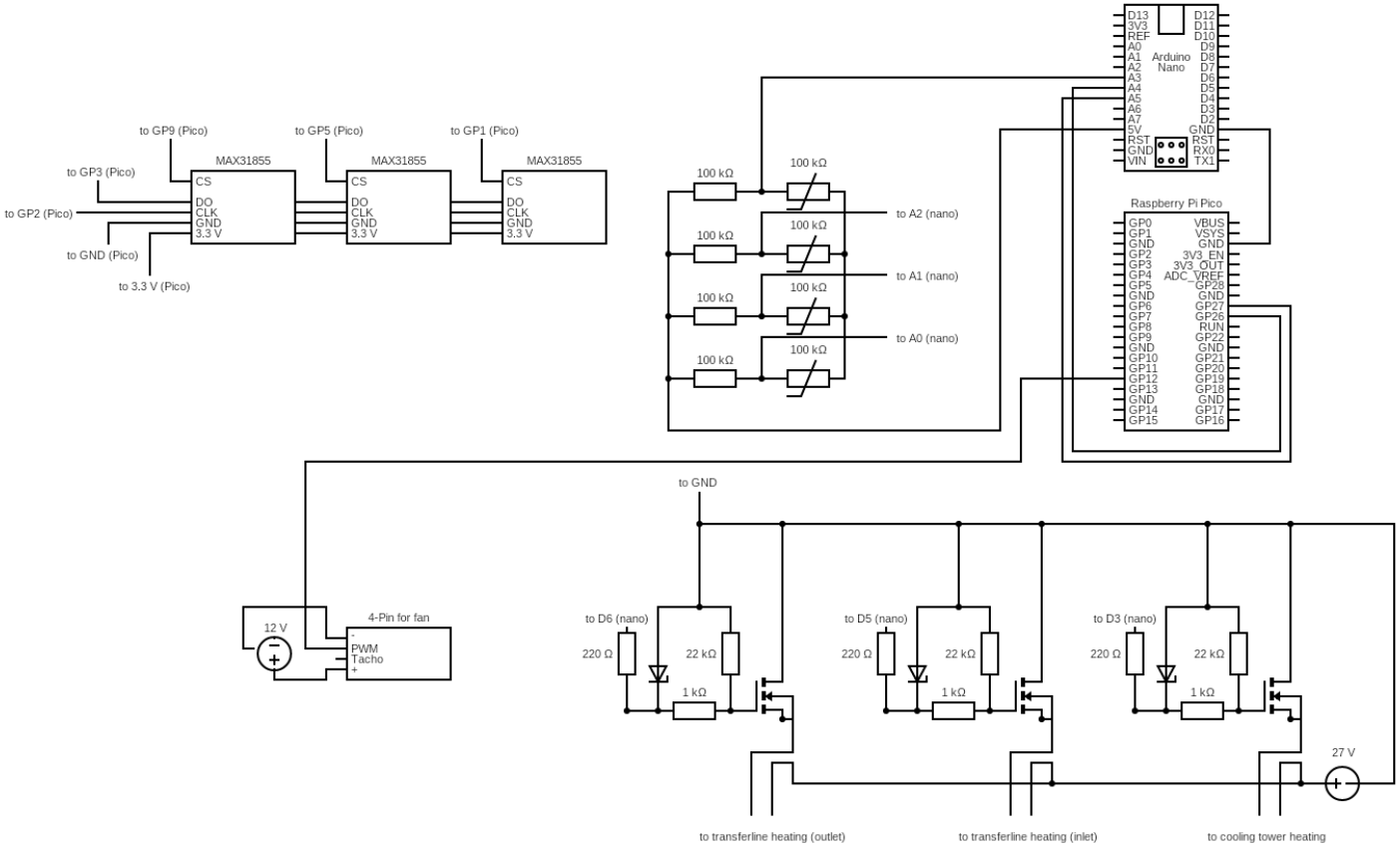

Figure 59: Circuit diagram of the circuit used for controlling the cooling tower.

```
#include <Wire.h>   //I2C-Library, e.g. for data-transmission from Slave-
Arduino to Master-Arduino
#include <PID_v1.h>     // PID File
//#include <PWM.h>        // File for PWM frequency variation

// V-probing: number of analog samples to take per reading
#define NUM_SAMPLES 20

int sum = 0;                    // sum of samples taken
unsigned char sample_count = 0; // current sample number
float voltage = 0.0;            // calculated voltage

// Section for setup of I2C-data-transmission

int T_0;      //thermocouple temperature 0 = inlet transfer temperature
int T_1;      //thermocouple temperature 1 = inlet temperature
int T_2;      //thermocouple temperature 2 = outlet temperature (at the moment
empty value)
int T_3;      //thermocouple temperature 3 = outlet transfer temperature
int I2Cdata[4];   //array that carries data
int I2Caddress_0 = 5;   //I2C address of the required Slave-Arduino

/////   User Set Variables for regular Use     /////

//Start delay
int start_delay = 5000;

// Set the target Temperatures  for the PID
double Temp_TransIn_Preheat = 210;               // inlet transfertemperature
(°C)
float Temp_Inlet_Preheat  = 25;     // Temperature of the hot Inlet for the
Preheating stage (°C)
float Temp_Outlet_Preheat = 25;    // Temperature of the Cold Outlet for the
Preheating stage (°C)
double Temp_TransOut_Preheat = 210;               // outlet
transfertemperature (°C)

// Max. PWM_Output to prevent too fast heating (Value should be between 1 and
255)
float max_TransIn_PWM = 16 ;   //14
float max_Inlet_PWM = 255;    //255
float max_Outlet_PWM = 254;   //254
float max_TransOut_PWM = 18;  //14

float min_Fan_PWM = 170;  //since PWM frequency is at its original value again
the Fan needs higher PWM-values to even start spinning = this value (170)

// Temperature Program Variables
```

```
const byte Number_Segments =
6;                                                                    //
Important! Number of Ramps in the Temperature Program after the Preheat Stage
float   SetTemp_TransIn[] =   { 200, 200, 200, 200, 200, 200,
200,  80,80,80,80,80};                  // Set the TransIn Temperatures at the
end each ramp in order (°C)
float   SetTemp_Inlet[]  =    { 200, 200, 200, 200,
200,  25,  25,   100,115,130,150,200};          // Set the Inlet Temperatures
at the end each ramp in order (°C)
float   SetTemp_Outlet[] =    { -40, 200, 200, 200,
200,  25,  25,   70,116,132,151,201};            // Set the Outlet
Temperatures at the end each ramp in order (°C)
float   SetTemp_TransOut[] =  { 200, 200, 200, 200, 200, 200,
200,  80,80,80,80,80};                  // Set the TransOut Temperatures at the
end each ramp in order (°C)
float   SetTime[]        =    { 0.05,0.01, 0.6, 1,
1,    0.1,  1,    1,1,0.8,0.2,1};               // Set the Duration of each
Ramp segment (min)

float MaxTemp = 250; // Maximum temperature allowed to be set into
SetTemp_Inlet[] and - Outlet[]. This is a Safety feature. Suggested Value:
300. (°C)

//  Loop Delays
int Total_Loop_delay = 500;          // Approximatly how long each loop should
take (ms).

// Data Output Variables
const bool DataRead_Excel = false;  // Variable for controlling the data
Output format.
                  // True:  MS Excel Data Streamer
                  // False: Arduino IDE Serial Monitor
const bool Monitor_Output = true;   // Should the Output PWM-Signal byte be
monitored in

// Signal Pins and Signal Variables
const byte ledPin1 = 13;           // End Preheat Signal LED Pin
const byte ButtonPin = 2;          // Pin for "End Preheat"-Signal button,
Note: must be digital pin 2 or 3 for Arduino Uno.

const byte ledPin2 = 12;           // Temperature Proximity Signal LED Pin
const float Temp_Prox = 1;         // In Preheat-Stage: LED on ledPin2 Lights
up, when both Temp. Sensors register Temperatures which are
// within Temp_Prox of their Setpoints

/////   User Set Variables for Development  /////

//PID Coefficients
double Kp0 = 2.0, Ki0 = 1.0, Kd0 = 1.0;    // Inlet Transferheater PID
Coefficients
```

```
double Kp1 = 5.0, Ki1 = 1, Kd1 = 0;     // Heating System PID Coefficients
double Kp2 = 4.0, Ki2 = 1, Kd2 = 0.1;    // Cooling System PID Coefficients
double Kp3 = 2.0, Ki3 = 1.0, Kd3 = 1.0;    // Outlet Transferheater PID
Coefficients

// Pin Positions of Digital Signal Outputs
int PIN_OUTPUT0 = 3;                  // the inlet transferheater Pin (hot
side)
int PIN_OUTPUT1 = 5;                  // the Heating System Transistor Pin
int PIN_OUTPUT2 = 9;                  // the Fan Pin
int PIN_OUTPUT3 = 6;                  // the outlet transferheater Pin (cold
side)

/////  Utility Variables, no adjustment required  /////

// Structure Utility Variables
volatile bool WaitState = true;                          // Variable for Ending
the Preheating Stage
void(* resetFunc) (void) = 0;                            // Prepares the Reset-
Function


// Temperature and Time Utility Arrays
float Array_Temp_TransIn[Number_Segments];        //
float Array_Temp_Inlet[Number_Segments];                 // These arrays take
their values from SetTemp_Inlet[], -Outlet[] and SetTime[]
float Array_Temp_Outlet[Number_Segments];                // But only
"Number_Segments" -members, Temperatures under MaxTemp and time in
milliseconds.
float Array_Temp_TransOut[Number_Segments];
float Array_Time[Number_Segments];

// Utility Time Variables
float Total_Time_min = 0;                          // Time since activation.
Millis() in minutes (min)
float Time_ms = 0;                              // Time since end of Setup (ms)
float Time_min = 0;                             //          -||-          (min)
float Time_Setup_ms = 0;                        // Setup duration         (ms)
float Time_Segment_ms = 0;                      // Counted time since the Start
of a certain Temperature Program Segment (ms)
float Time_PastSegments_ms = 0;                 // Time between Code Start the
start of a certain segment (ms)

// Calculated Utility Variables
double Ramp_TransIn;
double Ramp_Inlet;                              // Temperature Ramp of Inlet and
Outlet in °C/ms
double Ramp_Outlet;
double Ramp_TransOut;
```

```
// PID Variables and PID Instances
double Setpoint_Outlet;                         //Current Setpoint of the Outlet
and inlet
double Setpoint_Inlet;                          //    -||-
double Setpoint_TransIn;
double Setpoint_TransOut;

// Utility Variables for PID and 2 instances of PID-class objects
double Input0     = 30;
double Input1     = 30;                         //Current Setpoint of the Outlet
and inlet
double Input2     = 30;                         //    -||-
double Input3     = 30;
double Out0, Out1, Out2, Out3;
PID myPID0(&Input0, &Out0, &Setpoint_TransIn, Kp0, Ki0, Kd0, DIRECT);    //
inlet transferheater PID
PID myPID1(&Input1, &Out1, &Setpoint_Inlet, Kp1, Ki1, Kd1, DIRECT);    //
heater-MOSFET PID
PID myPID2(&Input2, &Out2, &Setpoint_Outlet, Kp2, Ki2, Kd2, REVERSE);   // Fan
PID
PID myPID3(&Input3, &Out3, &Setpoint_TransOut, Kp3, Ki3, Kd3, DIRECT);    //
outlet transferheater PID

int Output0, Output1, Output2, Output3;

// Temperature Registration
float TempC0;
float TempC1;
float TempC2;
float TempC3;
float TempNTC;

//-------------------------------------------------------------

void setup()
{ /*
      These Functions are for setting up different parts of the program:
      The Serial Monitor, the PIDs, the I²C-Communication for the Sensors,
      the changed PWM Frequency for the fan and Signal Input and Output pins
  */

  Serial.begin(9600);


  Wire.begin();  // Start I2C as Master for data-transmission

  pinMode(PIN_OUTPUT0,OUTPUT);
  pinMode(PIN_OUTPUT1,OUTPUT);
  pinMode(PIN_OUTPUT2,OUTPUT);
  pinMode(PIN_OUTPUT3,OUTPUT);
```

```
  myPID0.SetMode(AUTOMATIC);
  myPID1.SetMode(AUTOMATIC);
  myPID2.SetMode(AUTOMATIC);
  myPID3.SetMode(AUTOMATIC);

  pinMode(ledPin1, OUTPUT);
  pinMode(ledPin2, OUTPUT);
  digitalWrite(ledPin1, LOW);
  digitalWrite(ledPin2, LOW);
  pinMode(ButtonPin, INPUT_PULLUP);

  /* This Section is for preparing the Time and Temperature Arrays for use in
the Temperature Program. It feeds what is
     in the User-set Arrays (SetTemp_Inlet[], SetTemp_Outlet[] and SetTime[]
into Array_Temp_Inlet[],  --Outlet[] & -Time[]
     But only so many members as defined by Number_Segments
     Additionally, Temperatures are not allowed to be set at values over
MaxTemp. Doing so will have them overwritten by
     by MaxTemp and will print an Error-message.
     Times in Array_Time[] are converted to milliseconds.
  */

  for (int i = 0; i < Number_Segments; i++)

  { Array_Time[i] = SetTime[i] * 60 * 1000 ;

    if (SetTemp_TransIn[i] <= MaxTemp)
    { Array_Temp_TransIn[i] = SetTemp_TransIn[i] ;}

    else
    {
  Array_Temp_TransIn[i] = MaxTemp ;
      Serial.println("Error: An element of SetTemp_TransIn[] is greater than
MaxTemp and has been limited to MaxTemp");
    }

  if (SetTemp_Inlet[i] <= MaxTemp)
    { Array_Temp_Inlet[i] = SetTemp_Inlet[i] ;}

    else
    {
      Array_Temp_Inlet[i] = MaxTemp ;
      Serial.println("Error: An element of SetTemp_Inlet[] is greater than
MaxTemp and has been limited to MaxTemp");
    }

    if (SetTemp_Outlet[i] <= MaxTemp )
    {Array_Temp_Outlet[i] = SetTemp_Outlet[i] ;    }
```

```
    else
    {
      Array_Temp_Outlet[i] = MaxTemp ;
      Serial.println("Error: An element of SetTemp_Outlet[]is greater than
MaxTemp and has been limited to MaxTemp");
    }

  if (SetTemp_TransOut[i] <= MaxTemp )
    {Array_Temp_TransOut[i] = SetTemp_TransOut[i] ;    }

    else
    {
      Array_Temp_TransOut[i] = MaxTemp ;
      Serial.println("Error: An element of SetTemp_TransOut[]is greater than
MaxTemp and has been limited to MaxTemp");
    }

  }; //end For-loop

  if (Temp_TransOut_Preheat <= MaxTemp)
  {Setpoint_TransOut = Temp_TransOut_Preheat;}
  else
  {
  Setpoint_TransOut = MaxTemp;
  Serial.println("Error: Temp_Outlet_Preheat is greater than MaxTemp and has
been limited to MaxTemp");
  }

  if (Temp_Outlet_Preheat <= MaxTemp)
  {Setpoint_Outlet = Temp_Outlet_Preheat;}
  else
  {
  Setpoint_Outlet = MaxTemp;
  Serial.println("Error: Temp_Outlet_Preheat is greater than MaxTemp and has
been limited to MaxTemp");
  }

    if (Temp_Inlet_Preheat <= MaxTemp)
  {Setpoint_Inlet = Temp_Inlet_Preheat;}
  else
  {
  Setpoint_Inlet = MaxTemp;
  Serial.println("Error: Temp_Inlet_Preheat is greater than MaxTemp and has
been limited to MaxTemp");
  }

  if (Temp_TransIn_Preheat <= MaxTemp)
  {Setpoint_TransIn = Temp_TransIn_Preheat;}
  else
  {
```

```
  Setpoint_TransIn = MaxTemp;
  Serial.println("Error: Temp_Inlet_Preheat is greater than MaxTemp and has
been limited to MaxTemp");
  }

  // First Information Output to the Computer. Format dependant on the
monitoring Program
  if (DataRead_Excel == true) {                          // Output Via MS
Excel Datastreamer

    if (Monitor_Output == true) {                        // Monitoring Output
is activated
      Serial.println("Heating to set Temperatures...");
      Serial.println("TimeTotal,Time,TransIn-T,Inlet-T,Inlet-Setp.,Outlet-
T,Outlet-Setp.,TransOut-T,TransIn,Inlet,Outlet,TransOut");


      Serial.println("(min),(min),(deg. C),(deg. C),(deg. C),(deg. C),(deg.
C),(deg. C),(),(),(),()");
    }
    else {                                               // Monitoring Output
is deactivated
      Serial.println("Heating to set Temperatures...");
      Serial.println("TimeTotal,Time,TransIn-T,Inlet-T,Outlet-T,TransOut-T");
      Serial.println("(min),(min),(deg. C),(deg. C),(deg. C),(deg. C)");
    }
  } // End of Excel-Output branch


  else {                                                 // Output Via Arduino
IDE Serial Monitor

    if (Monitor_Output == true) {                        // Monitoring Output
is activated
      Serial.println("Heating to set Temperatures...");
      Serial.println("TimeTotal  Time  TransIn-T   Inlet-T   Inlet-
Setp.  Outlet-T   Outlet-Setp.  TransOut-
T      TransIn     Inlet    Outlet    TransOut    |Voltage");
      Serial.println("(min)     (min)    (°C)       (°C)      (°C)         (°C
)        (°C)         (°C)           ()          ()        ()        ()
 |(V) ");
    }
    else {                                               // Monitoring Output
is deactivated
      Serial.println("Heating to set Temperatures...");
      Serial.println("TimeTotal  Time  TransIn-T   Inlet-T   Outlet-
T   TransOut-T");
      Serial.println("(min)     (min)    (°C)       (°C)      (°C)      (°C)")
;
    }
```

```
  } // End of Serial Monitor Output Branch


 /*
     This program Segment runs the preheating stage. A while-loop containing
RunPID
     runs at the Temp_Inlet_Preheat & -Outlet- Temperature setpoints while
WaitState is "true".
     When the Button on ButtonPin is pressed, the interrupt is triggered and
the
     function ChangeState() switches Waitstate from true to false, ending the
Loop
     An LED is turned on to indicate this.
  */
  //attachInterrupt(digitalPinToInterrupt(ButtonPin), ChangeState, FALLING);
  while (WaitState == true)
  {
    RunPID();                                 // The actual PID running commands

    if (voltage > 3)
    {
      delay(start_delay);
      ChangeState();
    }

    //Serial.println("Step: Preheating "); // Additional Data Output of which
Step. Same for Excel and Serial Monitor.

    if ( (abs(TempC2 - Temp_Outlet_Preheat) < Temp_Prox) && (abs(TempC1 -
Temp_Inlet_Preheat) < Temp_Prox))
    {
      digitalWrite(ledPin2, HIGH);
    }

    else
    {
      digitalWrite(ledPin2, LOW);
    }

  } //End While-Loop


  digitalWrite(ledPin2, LOW);
  Time_Setup_ms = millis();   // Register Time Required for Setup
}


//-------------------------------------------------------------

void loop() {
```

```
  /* This part of the program runs the temperature ramp.
     It consists of a for loop containing a while loop.
     The for loop defines which segment (i.e. which element of the Arrays) is
being run
     The While loop runs the actual ramp.
  */

  for (int i = 0; i < Number_Segments; i++)
  {
    if (i == 0) // defines the current ramp
    {
    Ramp_TransIn = (Array_Temp_TransIn[i] - Temp_TransIn_Preheat) /
Array_Time[i];
    Ramp_Inlet = (Array_Temp_Inlet[i] - Temp_Inlet_Preheat) / Array_Time[i];
      Ramp_Outlet = (Array_Temp_Outlet[i] - Temp_Outlet_Preheat) /
Array_Time[i];
    Ramp_TransOut = (Array_Temp_TransOut[i] - Temp_TransOut_Preheat) /
Array_Time[i];
    }

    else
    {
    Ramp_TransIn =  (Array_Temp_TransIn[i] - Array_Temp_TransIn[i - 1]) /
Array_Time[i];
    Ramp_Inlet =  (Array_Temp_Inlet[i] - Array_Temp_Inlet[i - 1]) /
Array_Time[i];
      Ramp_Outlet = (Array_Temp_Outlet[i] - Array_Temp_Outlet[i - 1]) /
Array_Time[i];
    Ramp_TransOut =  (Array_Temp_TransOut[i] - Array_Temp_TransOut[i - 1]) /
Array_Time[i];
    }


    Time_Segment_ms = 0;
    Time_PastSegments_ms = millis();



    while ((millis() - Time_PastSegments_ms) < Array_Time[i])
    {
      Time_Segment_ms = millis() - Time_PastSegments_ms;
      Time_ms = millis() - Time_Setup_ms;
      Time_min = Time_ms / 60 / 1000;


      if (i == 0) {
    Setpoint_TransIn = Temp_TransIn_Preheat + Ramp_TransIn * Time_Segment_ms;
        Setpoint_Inlet = Temp_Inlet_Preheat + Ramp_Inlet * Time_Segment_ms;
        Setpoint_Outlet = Temp_Outlet_Preheat + Ramp_Outlet * Time_Segment_ms;
```

```
    Setpoint_TransOut = Temp_TransOut_Preheat + Ramp_TransOut *
Time_Segment_ms;
      }

      else {
    Setpoint_TransIn = Array_Temp_TransIn[i - 1] + Ramp_TransIn *
Time_Segment_ms;
        Setpoint_Inlet = Array_Temp_Inlet[i - 1] + Ramp_Inlet *
Time_Segment_ms;
        Setpoint_Outlet = Array_Temp_Outlet[i - 1] + Ramp_Outlet *
Time_Segment_ms;
    Setpoint_TransOut = Array_Temp_TransOut[i - 1] + Ramp_TransOut *
Time_Segment_ms;
      }


      RunPID();
      //Serial.print("Step: ");    Serial.println(i+1); // Additional Data
Output of which stage. Same for Excel and Serial Monitor




    } //End While Loop
  } //End For Loop


  //Serial.println("End of Temperature Program, Resetting The Arduino...");
  Serial.println();
  analogWrite(PIN_OUTPUT2, 0);   // Deactivates the Heating System while
waiting for the reset. Safety Feature.

  Blink();                       //Blink and Wait. Duration 1s. x3
  Blink();
  Blink();

  resetFunc();

  Serial.println("This is an Easter Egg. The Arduino should never print
this.");

} // End of Loop() // End of Code
```

```
//-------------------------------------------------------------
// Functions
//-------------------------------------------------------------

float ReadTemp(int Address)                // Function for getting Temperatures
from the NTC
{

  //Settings for NTC-Resistor

  int bitwertNTC= 0;
  long widerstand1=100000;                    //Widerstand des NTC-Widerstands
in Ohm
  int bWert =3950;                            // B- value of the NTC
  double widerstandNTC =0;
  double kelvintemp = 273.15;                 // 0°Celsius in Kelvin
  double Tn=kelvintemp + 25;                  //Temperature in Kelvin
  double TKelvin = 0;                        //calculated Temperature in °C
  double TempC = 0;

  //////NTC-Calculation_START/////////


  // read analog value
  bitwertNTC = analogRead(Address);
  // calculate resistance of the NTC
  widerstandNTC = widerstand1*(((double)bitwertNTC/1024)/(1-
((double)bitwertNTC/1024)));
  // calculate Temperature in Kelvin
  TKelvin =
1/((1/Tn)+((double)1/bWert)*log((double)widerstandNTC/widerstand1));
  // Temperature in °C
  TempC=TKelvin-kelvintemp;

  //////NTC-Calculation_END/////////

  return TempC;

} // End of ReadTemp()

void RunPID()
{
  v_probing();
  Wire.requestFrom(I2Caddress_0,4);

  I2Cdata[0]=Wire.read();
  I2Cdata[1]=Wire.read();
  I2Cdata[2]=Wire.read();
  I2Cdata[3]=Wire.read();
```

```
  T_0 = I2Cdata[0];
  T_1 = I2Cdata[1];
  T_2 = I2Cdata[2];
  T_3 = I2Cdata[3];

  Total_Time_min = float(millis()) / 60 / 1000;  // Time since Arduino turned
on or last reset

  if(WaitState == false){
  Time_ms = millis() - Time_Setup_ms;        // Count Time since Setup
  Time_min = (float(Time_ms)) / 60 / 1000;
  }

  //Calculate Output for the Inlet Transfer Heating System
  TempC0 = ReadTemp(A2);
  Input0 = TempC0 ;                    // Input for myPID0 is TempC0.
  myPID0.Compute();                    // Calculate Output0.
  Output0 = round(Out0)/255*max_TransIn_PWM;
  analogWrite(PIN_OUTPUT0, Output0);   // Send PWM-signal to heater-MOSFETs.

  //Calculate Output for the Heating System of the Cooling Tower
  TempC1 = T_0;
  Input1 = TempC1 ;                    // Input for myPID1 is TempC1.
  myPID1.Compute();                    // Calculate Output1.
  Output1 = round(Out1)/255*max_Inlet_PWM;
  analogWrite(PIN_OUTPUT1, Output1);   // Send PWM-signal to heater-MOSFETs.

  //Calculate Output for Cold End
  TempC2 = T_1;
  Input2 = TempC2 ;                   // Input for myPID1 is TempC1.
  myPID2.Compute();                   // Calculate Output1.
  Output2 = ((Out2/254)*(max_Outlet_PWM-min_Fan_PWM))+min_Fan_PWM;
  analogWrite(PIN_OUTPUT2, Output2);     // Send PWM-signal with changed
Frequency to Fan.

  //Calculate Output for the Outlet Transfer Heating System
  TempC3 = T_3;
  Input3 = TempC3 ;                    // Input for myPID3 is TempC3.
  myPID3.Compute();                    // Calculate Output3.
  Output3 = round(Out3)/255*max_TransOut_PWM;
  analogWrite(PIN_OUTPUT3, Output3);   // Send PWM-signal to heater-MOSFETs.

  TempNTC = ReadTemp(A1);




if (DataRead_Excel == true) {       // Output Via MS Excel Datastreamer
    Serial.print(Total_Time_min, 3);    Serial.print(",");
    Serial.print(Time_min, 3);          Serial.print(",");
```

```
    Serial.print(TempC0);                Serial.print(",");
    Serial.print(TempC1);                Serial.print(",");
    Serial.print(Setpoint_Inlet);        Serial.print(",");
    Serial.print(TempC2);                Serial.print(",");
    Serial.print(Setpoint_Outlet);       Serial.print(",");
    Serial.print(TempC3);                Serial.print(",");

    if (Monitor_Output == true) {      // Monitor Output PWM-Signals is
activated
      Serial.print(Output0);      Serial.print(",");
      Serial.print(Output1);      Serial.print(",");
      Serial.print(Output2);      Serial.print(",");
      Serial.print(Output3);      Serial.print(",");
      Serial.print(voltage);      Serial.println();
    }
    else {                               // Monitor Output PWM-Signals is
deactivated
      Serial.println("");                // New Line
    }

  }   // End if Excel-Readout Branch

  else {                                 // Output Via Arduino IDE Serial
Monitor
    Serial.print(Total_Time_min, 3);  Serial.print("    ");
    Serial.print(Time_min, 3);        Serial.print("    ");
    Serial.print(TempC0);             Serial.print("      |");
    Serial.print(TempC1);             Serial.print("       ");
    Serial.print(Setpoint_Inlet);     Serial.print("|      |");
    Serial.print(TempC2);             Serial.print("       ");
    Serial.print(Setpoint_Outlet);    Serial.print("|      ");
    Serial.print(TempC3);             Serial.print("    |||    ");

    if (Monitor_Output == true) {      // Monitor Output PWM-Signals is
activated
      Serial.print(Output0);        Serial.print("         ");
      Serial.print(Output1);        Serial.print("         ");
      Serial.print(Output2);        Serial.print("         ");
      Serial.print(Output3);        Serial.print("         ");
      //Serial.print(TempNTC);        Serial.print("         ");
      Serial.print(TempNTC);        Serial.println();
    }
    else {                               // Monitor Output PWM-Signals is
deactivated
      Serial.println("");                // New Line
    }
  }   // End if Serial Monitor-Readout Branch


  delay(Total_Loop_delay);
```

```
} // End of RunPID()

void ChangeState() {                //Function for changing the value
WaitState and triggering the start of the Temperature Program.
  //Activated by an Interrupt in the Preheating Stage
  WaitState = !WaitState;       //Change Waitstate from true to false
  digitalWrite(ledPin1, HIGH);  // Turn on an LED as a Signal.
}

void Blink() {
  digitalWrite(ledPin1, LOW);
  delay(500);
  digitalWrite(ledPin1, HIGH);
  delay(500);
}


void v_probing()
{
  // take a number of analog samples and add them up
    while (sample_count < NUM_SAMPLES) {
        sum += analogRead(A6);
        sample_count++;
        delay(10);
    }
    // calculate the voltage
    // use 5.0 for a 5.0V ADC reference voltage
    // 5.015V is the calibrated reference voltage
    voltage = ((float)sum / (float)NUM_SAMPLES * 5.015) / 1024.0;
    // send voltage for display on Serial Monitor
    // voltage multiplied by 11 when using voltage divider that
    // divides by 11. 11.132 is the calibrated voltage divide
    // value
    voltage = voltage*11.132;
    sample_count = 0;
    sum = 0;
    delay(0);
}
```